

Chapter xx

Bridge abutment mode of cement-mixed gravel backfill

Fumio Tatsuoka

Professor, Tokyo University of Science, Chiba, Japan

Masaru Tateyama

Research Engineer, Railway Technical Research Institute, Japan

Hifumi Aoki

Engineer, Japan Railway Construction Agency

Kenji Watanabe

Research Engineer, Railway Technical Research Institute, Japan

Abstract: This report describes a new type bridge abutment consisting of the backfill of geogrid-reinforced cement-mixed gravely soil and a thin RC parapet structure (i.e., a parapet) supporting a bridge girder, which was completed in 2003 for a new bullet train line in Kyushu, Japan. The backfill and the parapet are firmly fixed to each other with geogrid layers embedded in the cement-mixed backfill. This structure is very unique in that the backfill supports laterally the RC parapet, rather than exerting static and dynamic earth pressure on the back face of the parapet in comparison with the conventional type bridge abutment consisting of a relatively massive reinforced concrete structure supporting the backfill of uncemented soil. It is shown that the new type bridge abutment is very cost-effective. A series of model shaking table tests were performed to evaluate the seismic stability of conventional type bridge abutments as well as several new type bridge abutments including the one that was actually employed to construct the prototype one. Results from a series of drained triaxial compression tests on cement-mixed gravel are reported. It is shown that cement-mixed gravely soil should be mixed at the optimum water content for compaction energy used to construct the backfill. It is shown that the compressive strength of cement-mixed gravely soil increases considerably with compacted dry density. The design, in comparison to the one of the conventional type bridge abutment, and the staged construction procedure of the prototype bridge abutment are described. Results from field full-scale lateral loading tests on the abutment performed to ensure the design conditions are reported. The prototype bridge abutment performed very well showing highly integrated behaviour with very high connection strength between the backfill and the parapet.

1. INTRODUCTION

This paper reports the recent construction of a bridge abutment consisting of the backfill of geogrid-reinforced cement-mixed gravel and a thin RC facing structure (i.e., a parapet) supporting a bridge girder for a new bullet train line in Kyushu (the south-end major island of Japan), which was completed in 2003. This new type of bridge abutment (Figure 1) is unique in that the backfill supports laterally the parapet, rather than exerting static and dynamic earth pressure on the back face of the parapet, during static and seismic loading conditions.

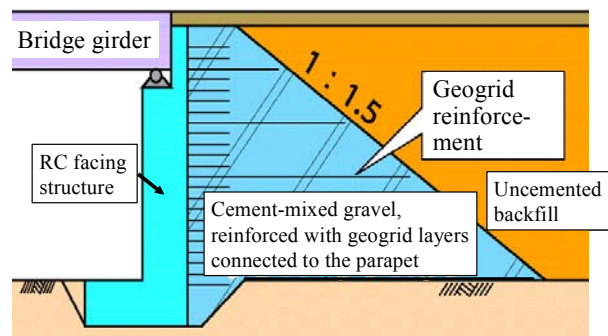


Fig. 1. A new type bridge abutment using backfill of cement-mixed gravel

The background for the development of this new type of bridge abutment is as follows. A great number of conventional type railway bridge abutments (Figure 2a) were seriously damaged with a large relative settlement between the abutment and the backfill by a number of previous major earthquakes in Japan, including the 1995 Hyogo-ken Nambu Earthquake (so called the Great Kobe Earthquake), as described by Tatsuoka et al. (1997c & d). Such a relative settlement as above could endanger safe train operation even when it is small, say 10 cm. To prevent this type of damage, in 1978, the Japan National Railway (presently several Japan Railway Companies) introduced such a new type of backfill as shown in Figure 2b: i.e., a triangle-shaped backfill zone immediately behind the abutment, called “approach block”, is constructed by well compacting a well-graded gravelly soil. However, a number of this type of bridge abutments did not perform satisfactorily during several major

earthquakes that took place subsequently. Figure 3 shows a typical case showing the above.

Most recently, the approach blocks for a number of bridge abutments for new bullet train lines were constructed by using a well-graded gravely soil mixed with cement to decrease as much as possible the settlement of the backfill relative to the RC abutment. However, as the approach block is not connected to the RC abutment, so the backfill is not designed to directly support the RC abutment, the dimensions of the RC abutment are not reduced substantially by using the backfill comprising cement-mixed gravely soil.

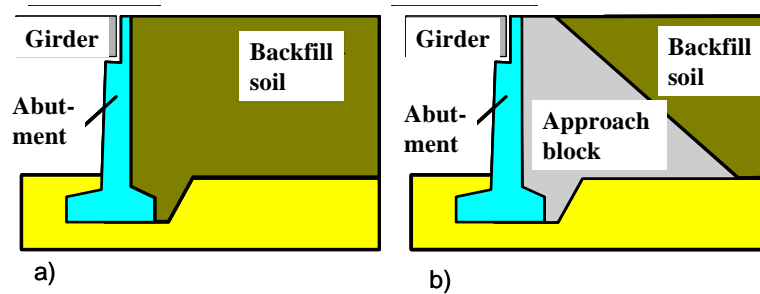


Fig. 2. Typical conventional bridge abutment types for railway; a) most conventional type (model 1 in the shaking table tests described later in this chapter); and b) a new type structure introduced in 1978 (model 2 in the shaking table test) (Watanabe et al., 2002).

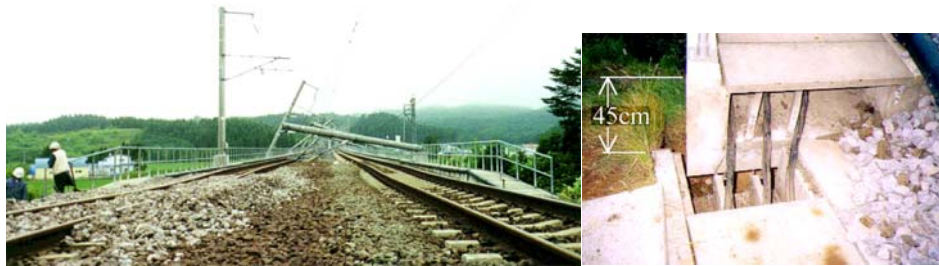


Fig. 3. A settlement of the backfill relative to an abutment, Arikawa bridge, Tsugaru-Kaikyo Line, East Japan Railway, Hokkaido Nansei-oki Earthquake, 12 July 1993 (by the courtesy of Railway Technical Research Institute, Japan).

In view of the above, the Railway Technical Research Institute, Japan, the University of Tokyo and the Japan Railway Construction Public Corporation started a long-term joint research project in 1997 aiming at the development of new seismic-resistant and cost-effective types of bridge abutment. Eventually, the following two types were proposed and studied as feasible types:

- 1) The backfill consists of a zone of geogrid-reinforced cement-mixed well-graded gravelly soil, which should be well compacted, immediately behind the full-height rigid facing structure supporting a bridge girder (Figure 1).
- 2) The backfill is geogrid-reinforced well-compacted well-graded gravelly soil that is supporting a bridge girder (Figure 4). The backfill is preloaded and prestressed by using tie rods of which the top ends are fixed to the top reaction block placed on the crest of backfill by using a special connection device (called the ratchet system; Shinoda et al. 2002b; Uchimura et al., 2003).

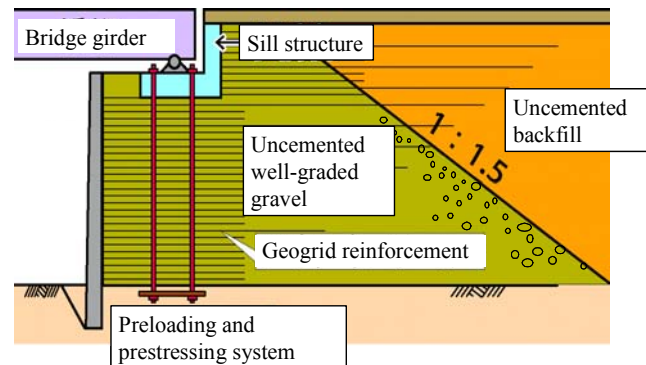


Fig. 4. A new type bridge abutment using preloaded and prestressed geogrid-reinforced backfill (Tatsuoka et al., 1997b, c; Nakarai et al., 2002; Shinoda et al., 2003a, b; Uchimura et al., 2003).

With both newly proposed types of bridge abutment, the geogrid layers that are embedded in the backfill to prevent separation into parts are connected to the back of the parapet. The first purpose of this connection is to restrain the settlement of the approach block relatively to the parapet. As shown below, the connection is also essential to maintain a high integrity of the abutment structure, in particularly under severe seismic loading conditions. By this connection, the steel-reinforced concrete facing structure (i.e., the parapet) becomes a continuous beam that are supported at a large number of supports with a small spacing and therefore it becomes substantially less massive than the conventional type RC bridge abutment. Moreover, as the parapet is constructed after the backfill is completed by a staged construction procedure and the stability of the complete parapet is controlled by the bearing capacity of ground immediately below the parapet to a much less extent than the conventional type bridge abutments, it is usually unnecessary to support the parapet with piles unless

the supporting ground is soft. For these reasons, this new type bridge abutment is considerably much more cost-effective than the conventional type ones.

In the following, first the results from a series of shaking table tests on small-scale models performed to develop the first new type (Figure 1) are **summarized**. Then, the results from a series of drained TC tests on cement-mixed gravelly soil that were carried out to determine the mixing proportion and the compaction details of cement-mixed gravelly soil are presented. Finally, the design and construction of the first prototype structure and results from field full-scale loading tests are reported.

2. SHAKING TABLE TESTS

2.1 General

A series of model shaking table tests were performed to compare the seismic stability of the new type abutment (Figure 1) in comparison with that of the conventional type ones (Figure 2); and to ensure whether the new type abutment can behave satisfactorily even during very high-intensity seismic load (so-called Level 2 design seismic load, the highest seismic load level to be accounted for in the Japanese aseismic design codes and standards) (Watanabe et al., 2002).

Table 1 Abutment models tested (Watanabe et al., 2002).

Model name	Backfill	Reinforcement	Input motion	Width of footing for RC facing
Model 1 (Conventional)	No approach block (Toyoura sand, $D_r = 75\%$)	No	Sinusoidal wave & Kobe wave	390 mm
Model 2 (Conventional)	With approach block of dry gravel ($\gamma_d = 1.9 \text{ g/cm}^3$)	No	Sinusoidal wave	390 mm
Model 3 (Conventional)	With approach block of cement-mixed gravel	No (backfill and facing unconnected)	Sinusoidal wave	390 mm
Model 4 (New type)	With approach block of cement-mixed soil	Yes (backfill and facing connected)	Kobe wave followed by sinusoidal wave	290 mm
Model 5 (New type)	With approach block of cement-mixed soil	Yes (backfill and facing connected)	Kobe wave followed by sinusoidal wave	200 mm

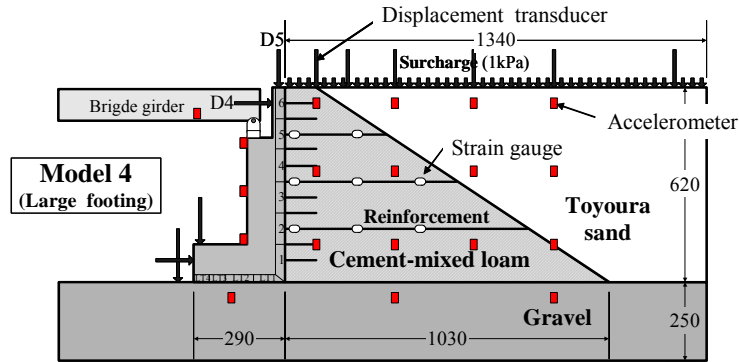


Fig. 5. Cross-sections of reinforced abutment with cement treated backfill (Model 4) (Watanabe et al., 2002).

2.2 Test Procedures

Models of bridge abutment. The following five types of abutments were investigated (Table 1):

Model 1: the most conventional type with uncemented backfill of ordinary soil type (Figure 2a).

Model 2: one of the conventional types with an approach block of well-compacted uncemented well-graded gravelly soil (Figure 2b).

Model 3: the latest conventional type with an approach block that is well-compacted cemented well-graded gravelly soil that is not reinforced with geogrid reinforcement layers (so the backfill and the parapet are not connected to each other) (Figure 2b).

Models 4 & 5: a new type with an approach block of well-compacted cemented well-graded gravelly soil that is reinforced with geogrid reinforcement layers connected to the back of the parapet (Figure 1), having different widths of the footing for the parapet.

The parapet of these models was made of aluminum. The height was 620 mm having a footing base with a width of 390 mm (Models 1 – 3), 290 mm (Model 4) and 200 mm (Model 5). Figure 5 shows the details of Model 4. The parapet model supported a relatively heavy model bridge girder with a weight of 200 kg through a hinge support on its top of the parapet (i.e., the fixed support). So, full dynamic lateral load of the girder was activated to the parapet. The unreinforced backfill of Model 1 was made by pluviating through air air-dried fine sand (Toyouura sand) from a sand hopper at a constant falling height to have a relative density D_r equal to 75 %. The approach block of Model 2 was made by compacting a well-graded gravelly soil ($U_c=10.7$; $D_{50}= 1.1$ mm, $D_{max}=5.0$ mm and a

finer content = 5.2 %; a water content = 5 %) to a dry density of 1.9 g/cm³. Despite that the actual approach block of this abutment type (also of the new types) is made of cement-mixed well-graded gravel, the model approach block of Model 3 was made of a cement-mixed loam having an unconfined compressive strength of 200 kN/m² considering the model similitude.

Models 4 and 5, which simulated the new structural types of bridge abutment, had a triangle-shaped approach block made of cement-mixed loam (the same as that of Model 3) that was reinforced with geogrid reinforcement layers connected to the back face of the parapet. The parapet directly supported the model bridge girder at its top. The footing base of the parapet was either relatively wide (Model 4) or relatively narrow (Model 5). The model geogrid was a grid made of 0.2 mm-thick and 3 mm-wide phosphor-bronze strips that were soldered to each other with a center-to-center spacing of 50 cm and 100 cm in the transversal and axial directions. The tensile force in the model reinforcement was measured by using electric-resistant strain gauges attached to the central strip at three levels. The stiffness of this model reinforcement was larger than actual polymer geogrids when considering the model similitude.

The model ground, supporting the model walls, was made by compacting an air-dried gravelly soil ($U_c = 12.1$; $D_{50} = 10.0$ mm, $D_{max} = 32.0$ mm and a finer content = 2.0 %) to a dry density of 1.9 g/cm³. The dynamic response of the abutment and backfill was measured with a number of displacement transducers and accelerometers (Figure 5). **The dynamic earth pressure and dynamic subsoil reaction acting on, respectively, the back face of the parapet and the bottom of the base footing of the parapet was measured with a number of two-component load cells measuring normal and shear forces (Figure 5).**

Dynamic loading at the shaking table. Models 1, 2 and 3 were subjected to a series of uniform sinusoidal wave, each comprising 50 waves while lasting for 10 seconds at a frequency of 5 Hz. The amplitude of horizontal acceleration at the shaking table, a_{max} , was increased step by step from the initial value of 50 gals with an increment of 50 gals until the displacements of the abutment became considerably large. Models 1, 4 and 5 were subjected to the time history of horizontal ground acceleration recorded at the Kobe Marine Meteorological Observation Station during the 1995 Hyogo-ken Nambu Earthquake. The predominant frequency of

this input motion had been adjusted to 5 Hz accounting for the model similitude. The table maximum amplitude, a_{max} , was increased step by step with an increment of 100 gals from 100 gals to 1,400 gals. In the tests on Models 4 and 5, the models did not reach ultimate failure even when the a_{max} value reached 1,400 gals. Therefore, subsequently sinusoidal waves were applied to these models stepwise increasing the a_{max} value from 100 gals with an increment of 100 gals until the models exhibited ultimate failure.

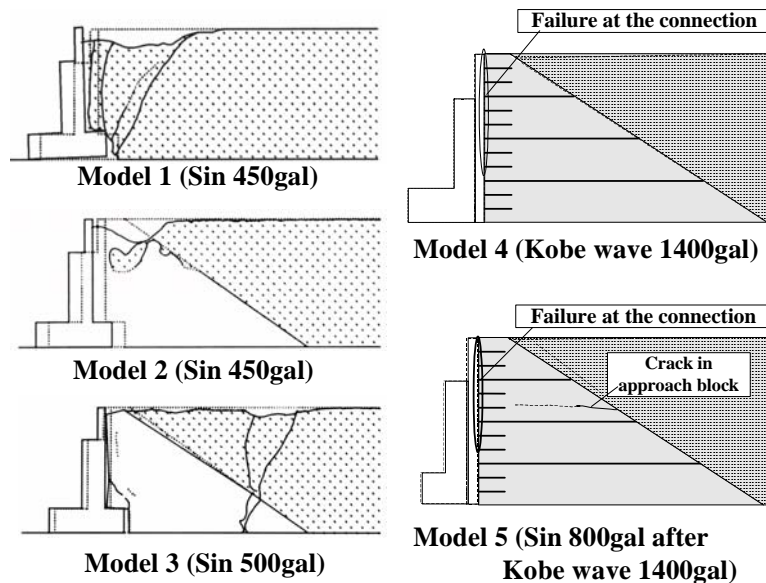


Fig. 6. Deformations of models after shaking table tests (Watanabe et al., 2002).

2.3 Test results and discussion

Models 1, 2 and 3. Figure 6 shows the failed models, observed after the respective test. Figures 7a and 7b show the residual displacements at the top of the parapet plotted against the maximum table acceleration, a_{max} , for all the models. The following trends of behaviour may be seen from these figures:

- 1) The deformation of Model 1 when the a_{max} value of sinusoidal motion became 450 gals was very large, showing ultimate failure with a fully developed single major failure plane in the backfill.
- 2) Model 2 also exhibited brittle failure when the a_{max} value of sinusoidal motion became 450 gals, showing very large deformation of the approach block of gravel, in particular at the upper part.

- 3) The deformation, in particular the settlement at the crest of the approach block, of Model 3 when the a_{max} value of sinusoidal motion became 450 gals was much smaller than that of Models 1 and 2. Despite the above, when the a_{max} value became 500 gals, the parapet started separating from the approach block, exhibiting a high dynamic response, because of no connection between them. Several major cracks developed in the approach block of Model 3, resulting into a loss of structural integrity as a bridge abutment.

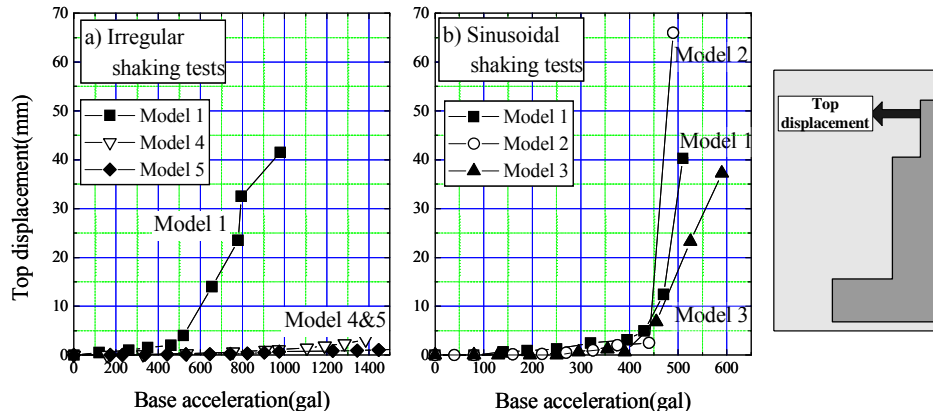


Fig 7. Residual displacements at the top of model abutment; a) irregular (Kobe wave); and b) sinusoidal table motion (Watanabe et al., 2002).

These results clearly indicate that the seismic stability of these three conventional types of bridge abutment when subjected to Level II seismic load is insufficient. The test results also suggest that the seismic stability of abutment can be increased by taking the following three measures:

- 1) By **constructing** the approach backfill using a stiffer material such as cement-mixed gravel soil, the backfill would exhibit substantially smaller settlements immediately behind the parapet.
- 2) By arranging horizontal reinforcement layers in the cement-mixed soil backfill, the development of major cracks in the zones where the tensile stress exceeds the tensile strength of cement-mixed soil could be effectively prevented.
- 3) By connecting the reinforcement layers to the back of the parapet that directly supports a bridge girder, relative settlements between them could be efficiently prevented while ensuring a high integrity of the whole abutment structure.

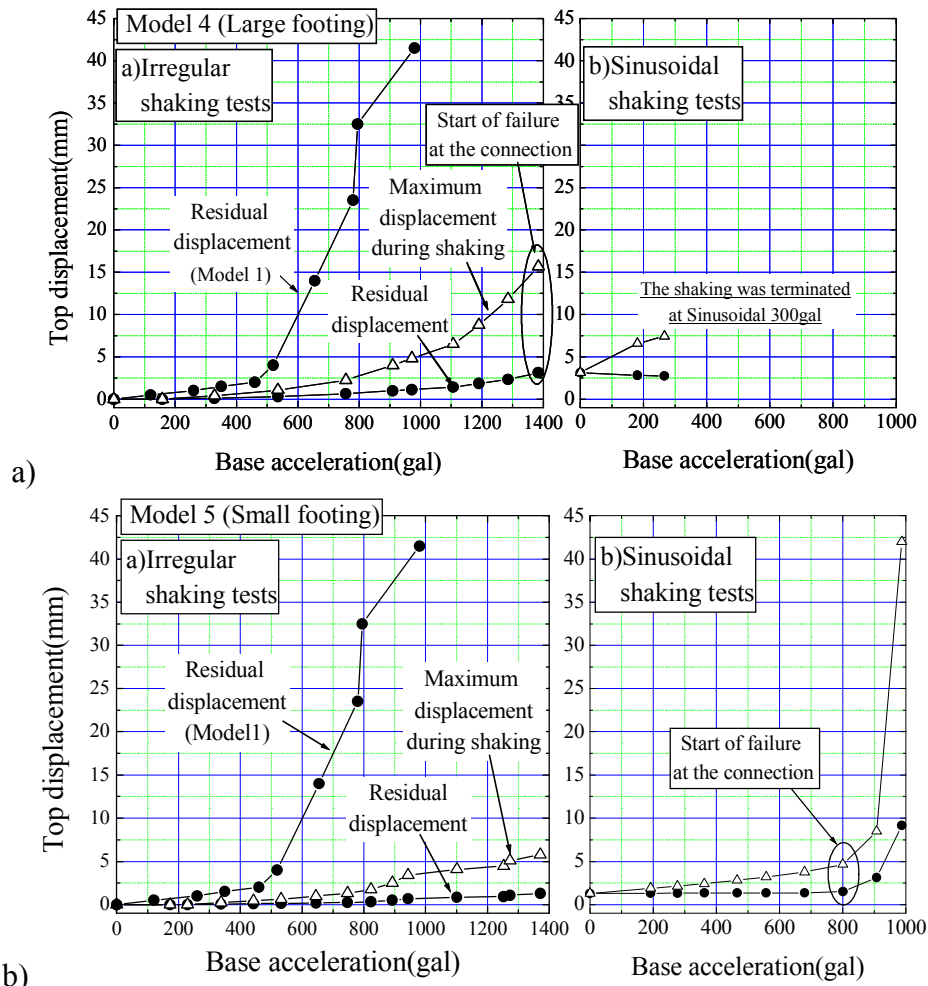


Fig. 8. Displacement at the top of model abutment of a) Model 4; and b) Model 5, compared to that of Model 1 (Watanabe et al., 2002).

Models 4 and 5 (simulating the proposed new types of bridge abutment). Eleven layers of grid reinforcements were arranged horizontal inside the approach block of cement-mixed soil with the ends connected to the back face of the parapet (Figure 5). Figures 8a and 8b show the relationships between the maximum and residual displacements recorded at the top of the parapet and the maximum table acceleration, a_{max} , when subjected to a) irregular waves and b) subsequently sinusoidal input waves. In these figures, the residual displacement at the top of the parapet of Model 1 is also presented as the reference. The following trends of behaviour may be seen from Figures 6, 7 and 8:

- 1) Models 4 and 5 were substantially more stable than Model 1 (i.e., the most conventional type abutment).
- 2) With Model 4, the tensile rupture of the connection between the reinforcement and the parapet started when the a_{max} value of irregular waves became 1,400 gals. This phenomenon was also noted by a sudden change in the reading of tensile strain at the respective reinforcement layer. With Model 5, it took place when the a_{max} value of sinusoidal wave became 800 gals, after having been subjected to a series of irregular motion.
- 3) The connection failure started earlier with Model 4 (with a wider footing) than with Model 5 (with a narrow footing). This unexpected trend of behaviour was due likely to larger relative vertical displacements at the interface between the approach block and the parapet with Model 4 because of a larger footing width (Figure 9). The fact that Model 5 (with a narrow footing) was more dynamically stable than Model 4 (with a wider footing) can be attributed to that the back-fill is more stable than the parapet, particularly under dynamic loading conditions.

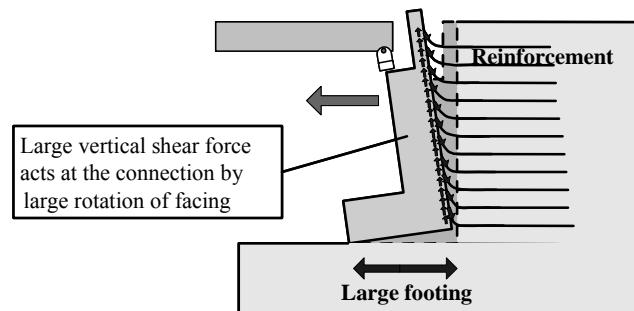


Fig. 9. Schematic diagram illustrating shear force acting at the connection of reinforcement, Model 4 (Watanabe et al., 2002).

These model test results indicate the essential importance of sufficiently high connection strength between the reinforcement and the parapet for a high seismic stability of this type of abutment structure. With a prototype of Model 5 bridge abutment, the connection strength between the reinforcement layers of a polymer geogrid and a full-height rigid facing (i.e., a parapet) was confirmed by performing full-scale lateral loading tests as described later in this chapter.

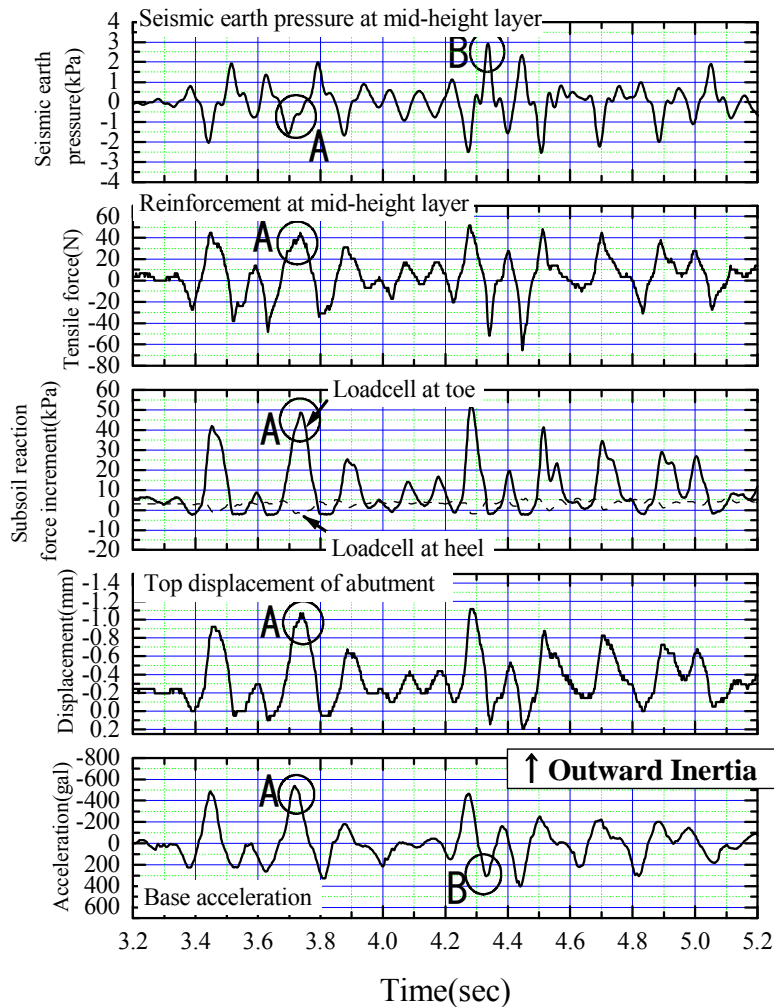


Fig. 10. Typical time histories of several measured physical quantities, Model 4 (irregular shaking, $a_{max} = 539$ gal) (Watanabe et al., 2002).

Dynamic disturbing force and resistance. Figure 10 shows the time histories of the following physical quantities when Model 4 was subjected to an irregular wave with $a_{max} = 539$ gals (see Figure 5 for the measuring points):

- 1) the dynamic component of the earth pressure acting on the back of the parapet;
- 2) the dynamic component of the reinforcement tensile force activated at a place adjacent to the back of the parapet;

- 3) the dynamic component of the vertical normal force acting at the toe and heel parts of the footing base of the parapet (note the normal and shear forces acting on the footing base were measured separately at four parts);
- 4) the dynamic component of the lateral displacement at the top of the parapet; and
- 5) the input horizontal acceleration at the shaking table.

The following trends of behaviour may be seen from this figure:

- 1) At the dynamically active earth pressure state (i.e., when the dynamic component of the lateral displacement at the top of the parapet was directing outwards as denoted *A* in Figure 10), the increasing resisting components were; a) the reacting vertical normal force near the toe of the footing base; and b) the tensile force in the reinforcement. On the other hand, until this state, the vertical contact force near the heel of the footing had already largely decreased, indicating an overturning displacement mode of the parapet.
- 2) At the dynamically active earth pressure state, the dynamic component of the earth pressure activated at the back face of the parapet exhibited the minimum value, showing that the parapet was dynamically less stable than the backfill. On the other hand, the maximum earth pressure was attained at the dynamically passive earth pressure state (as denoted *B* in Figure 10). With this type of bridge abutment, therefore, sufficiently high connection strength between the parapet and the reinforcement is essential for a high seismic stability at the dynamically active earth pressure state. These trends of dynamic earth pressure are opposite to those assumed in the conventional seismic design of conventional type retaining walls, in which the dynamic component of the active earth pressure becomes the maximum, which destabilizes the retaining wall.

Effects of the width of footing. Figure 11 shows the relationships between the maximum resistant moment acting at the footing base of the parapet defined about the heel of the footing base and the rotation angle of the parapet at each shaking stage using irregular waves for Models 4 and 5. Figure 12 shows the corresponding relationships between the base acceleration and the reinforcement tensile force activate adjacent to the back of the parapet (see Figure 5). It may be seen from these figures that the resistance moment acting at the footing base was larger with Model 4 (having a wider footing) than with Model 5 (having a narrower footing),

whereas the opposite was true with the reinforcement tensile force at the connection.

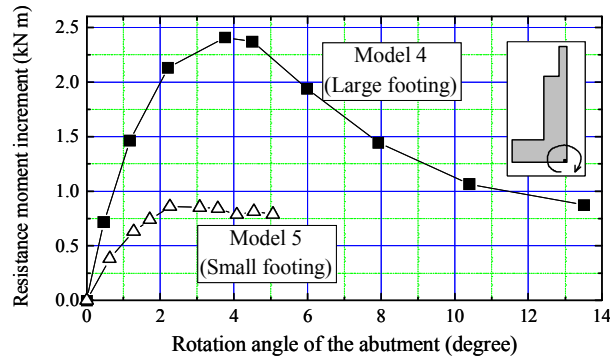


Figure 11 Relationships between rotation angle of parapet and resistance moment about the heel of the base of parapet resulting from the reacting vertical normal force of subsoil (Watanabe et al., 2002).

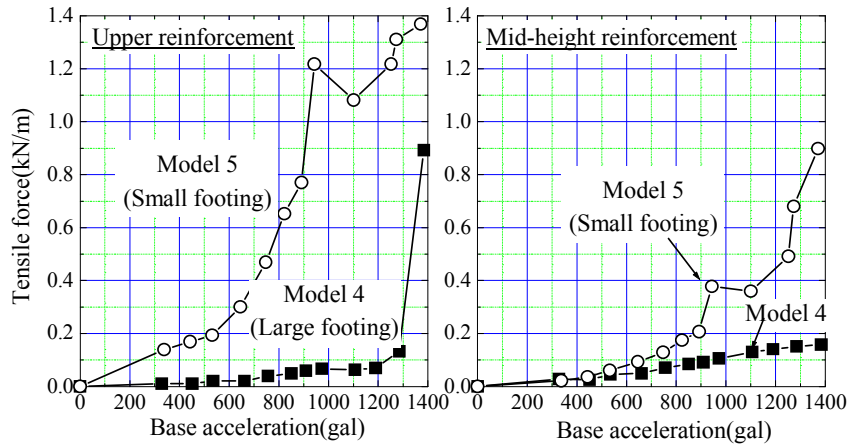


Fig. 12 Relationships between base acceleration and tensile force in; a) upper reinforcement; and b) mid-height reinforcement, Models 4 & 5 (Watanabe et al., 2002).

That is, with Model 5, the major resisting force was the tensile force at the connection between the parapet and the reinforcement. The maximum reinforcement tensile force consistently increased with an increase in the base acceleration, whereas the resisting moment acting at the footing base started decreasing with an increase in the base acceleration when the rotating angle of the footing base reached a certain value, associated with the start of failure in the ground supporting the footing. Due to such different resisting mechanisms, Model 5 was more stable than Model 4. With Model 5, larger connection force resulted in larger tensile force in

the reinforcement with larger load transmitted from the parapet to the cement-mixed soil approach block, which resulted in the development of a horizontal crack in the approach block (Figure 6). This type of crack did not develop in Model 4.

The test results presented above suggest that, by making sufficiently high the connection strength at the reinforcement layers and the parapet with sufficiently high strength of the backfill material of the approach block, the size of the base of the footing for the parapet of prototype structures can be made rather small as Model 5, which makes this type of abutment considerably cost-effective.

2.4 Summary of the model shaking table tests

The following conclusions can be derived from the test results of the model shaking table tests presented above:

- 1) The seismic stability of several conventional types of railway bridge abutment is not sufficiently high.
- 2) To increase the seismic stability of bridge abutment, it is efficient and cost-effective to construct an approach block using cement-mixed gravely soil that is reinforced with geogrid layers connected to the back face of a full-height rigid facing (i.e., a parapet) supporting a bridge girder.
- 3) A sufficiently high strength of the connection between the reinforcement layers and the parapet is essential not only to restrain the settlement of the backfill relative to the parapet but also to ensure a high dynamic stability of the parapet, which is less stable than the approach block.

3. STRENGTH OF CEMENT-MIXED GRAVEL

3.1 Background

It is necessary to evaluate the deformation and displacements of the concerned structure in addition to the safety factor against the ultimate failure of the structure both at working loads and under severe seismic loading conditions. To this end, the strength and deformation characteristics of cement-mixed gravely soil were evaluated by performing a series of consolidated drained triaxial compression (CD TC) tests as described below. At the same time, relevant mixing proportion of components as well

as relevant construction method was sought to achieve as high as strength per unit cost of cement-mixed gravel. A high cost-effectiveness is essential for the construction of this type of structure to become one of the standard construction methods for railway as well as highway structures.

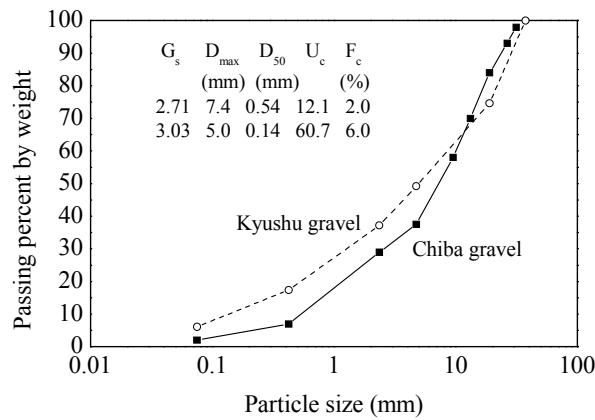


Fig. 13 Grading curves of two types gravels tested by large CD TC tests (Watanabe et al., 2003a).

Cement-mixed gravelly soil (CMG) has been used to construct large dams (i.e., the roller compacted dam concrete; e.g., Hansen & Reinhardt, 1990; Schrader 1996). However, only a limited amount of research has been performed on the use of CMG in ordinary but critical civil engineering structures requiring a high stability and allowing limited deformation, such as railway and highway bridge abutments. In the present study, a series of CD TC tests were performed on cement-mixed specimens of two types of well-graded quarry gravelly soils, which are typical of those used in the field (Figure 13). The first type was a crushed sandstone from a quarry (called Chiba gravel), which have been often used to study the strength and deformation properties of gravel at the University of Tokyo (e.g., Jiang et al., 1999). The other one was a crushed gabbro from another quarry (called Kyushu gravel), which was used as the backfill of a prototype of the new type bridge abutment explained later in this chapter. The effects of compacted dry density, moulding water content and gravel type on the strength and deformation characteristics of cement-mixed gravel were mainly investigated. The effects of grading characteristics were investigated to a limited extent. In addition, the strength characteristics of cement-mixed gravel were compared with those of uncemented original gravel. The effects of moulding water content and grading characteristics of gravel evaluated by CD TC tests using smaller specimens

(7.5 cm in diameter and 15 cm high) of model Chiba gravel are reported in Lohani et al. (2004) and Kongsukprasert et al. (2005). The effects of stress condition during curing on the strength and deformation characteristics evaluated also by CD TC tests using model Chiba gravel are reported in Kongsukprasert and Tatsuoka (2003).

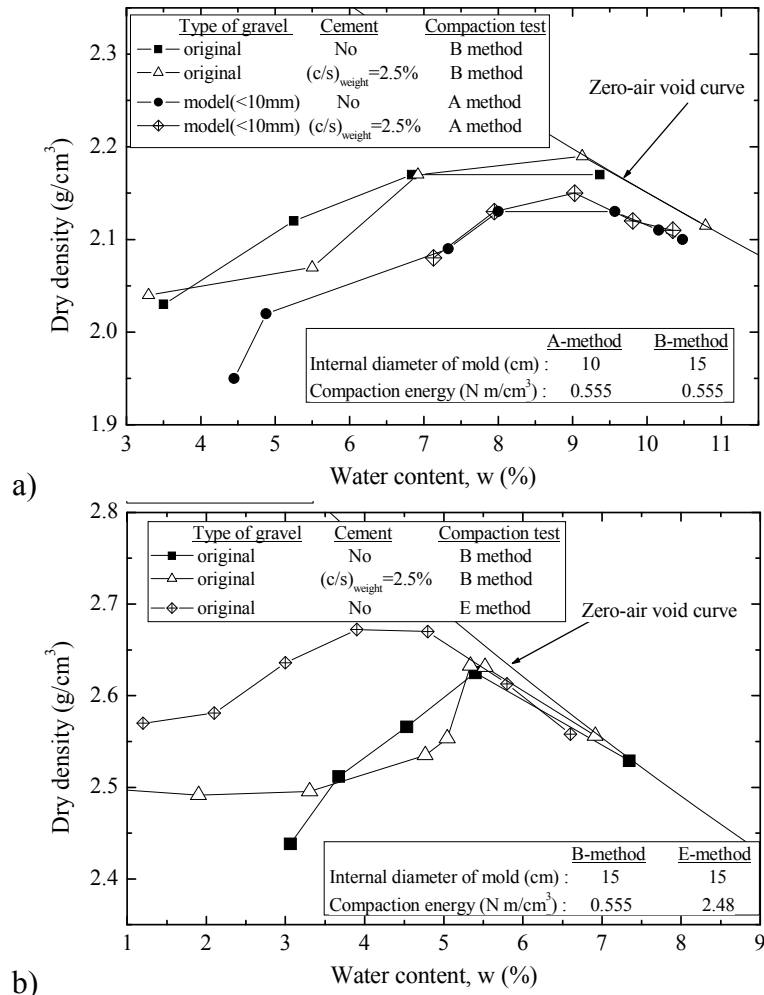


Fig. 14 Results of compaction tests; a) Chiba gravel; and b) Kyushu gravel (Watanabe et al., 2003a).

3.2 Testing apparatus and preparation of specimens

Gravel type and specimen preparation. Figure 14a shows the compaction curves of cement-mixed and uncemented specimens of the original Chiba gravel and the one obtained by removing particles larger than 10

mm (i.e., model Chiba gravel) obtained by the standard compaction tests. Figure 14b is similar results for the original Kyushu gravel. The sizes of mould and compaction energy levels used in these compaction tests are listed in these figures. It may be seen that the respective compaction curve of cement-mixed gravel is nearly the same as the corresponding one of uncemented gravel for these three types of gravel.

Table 2 List of specimen types tested (Watanabe et al., 2003a).

Specimen types	Dry density (g/cm ³)	Confining pressure (kPa)	Water content (%)	Cement/gravel ratio by weight; $W_{\text{cement}}/W_{\text{gravel}}$ (%)	Cement/gravel ratio by volume; $V_{\text{cement}}/V_{\text{gravel}}$ (%)	Size of specimen (mm)
Chiba (cement-mixed)	1.8, 2.0, 2.2	0, 20, 50	3.5, 5.0, 8.7, 10.5	2.5	6.78	ϕ 200* H400
Model Chiba (D < 10 mm) (cement-mixed)	2.0	20	8.7	2.5	6.78	ϕ 200* H400
Chiba (without cement)	1.8, 2.0, 2.2	0, 20, 80	4.0	-	-	ϕ 300* H600
Kyushu (cement-mixed)	2.41, 2.56, 2.64	0, 20, 50	4.35	2.5	7.58	ϕ 150* H300
Kyushu (without cement)	2.41, 2.56, 2.64	0, 20, 50	4.35	-	-	ϕ 200* H400

Table 2 lists five types of specimens prepared for the CD TC tests. The TC specimens were 20 cm in diameter and 40 cm high with cement-mixed Chiba gravel; and 30 cm in diameter and 60 cm high with uncemented Chiba gravel. To investigate the effect of grading characteristics on the strength and deformation characteristics of cement-mixed gravel, TC tests were performed also on cement-mixed specimens of model Chiba gravel. The specimens were 20 cm in diameter and 40 cm high. The TC specimens of cement-mixed Kyushu gravel were 15 cm in diameter and 30 cm high, which was because the strength of cement-mixed Kyushu gravel specimens with a diameter of 20 cm exceeded the capacity of the loading system. The specimens of Kyushu gravel without cement-mixing were 20 cm in diameter and 40 cm high. Throughout the present study, a fixed cement/gravel ratio by weight ($W_{\text{cement}}/W_{\text{gravel}}$) equal to 2.5 % was used as a typical value employed in the field.

The cement-mixed specimens were prepared by manual vertical compaction in about 6 or 12 sub-layers with a thickness of each sub-layer of 50 mm for all the specimens. Three ratios of compacted dry density to the respective maximum dry density attained by using compaction energy of 0.555 N m/cm^3 (for the compaction curves of cement-mixed gravel presented in Figure 14) were prepared, which were around 80 %, 90 % & 99 % for Chiba gravel and 91 %, 97 % & 100 % for Kyushu gravel. The moulding water content was basically 5 % (dry of optimum) and 8.7 % (optimum) with Chiba gravel, while it was 4.35 % (optimum for compaction by E-method and slightly dry of optimum for compaction by B-method) with Kyushu gravel. In order to investigate more in detail the effect of moulding water content on the strength characteristics, the moulding water content was varied between 3.5 % and 12 % with keeping the dry density constant (2.0 g/cm^3) with model Chiba gravel. The moulding water content was 4 % with uncemented Chiba gravel and 4.35 % with uncemented Kyushu gravel. The compacted cement-mixed specimens were cured for 7 days under the atmospheric pressure at constant water content before setting in the triaxial apparatus.

Triaxial test apparatus. All the CD TC tests were performed using a large triaxial testing apparatus at the Railway Technical Research Institute (Figure 15). The apparatus is able to control the axial displacement to an accuracy of less than $1 \mu\text{m}$ (Kohata et al., 1999). The axial load was measured with a load cell set inside the triaxial cell. The axial compression of specimen was measured externally with a pair of proximeters set at the specimen cap and locally with a pair of local deformation transducers (LDTs; Goto et al., 1991) that were set at the side face of specimen. The lateral deformations of specimen were measured by using three pairs of proximeters arranged at three elevations ($5/6$, $3/6$ and $1/6$ of the specimen height from the bottom), which were free from the effects of membrane penetration in these CD TC tests in which the effective confining pressure was kept constant.

The specimens were initially isotropically compressed to the prescribed confining pressure, σ_c' , and then sheared in drained TC at a constant axial strain rate of 0.01 %/min under constant σ_c' until the axial strain became 15 %. Three axial unload-reload cycles with a small axial strain amplitude were applied at various deviator stresses during other-

wise monotonic loading to evaluate the equivalent elastic vertical Young's modulus (E_{eq}) and Poisson's ratio (ν_{vh}).

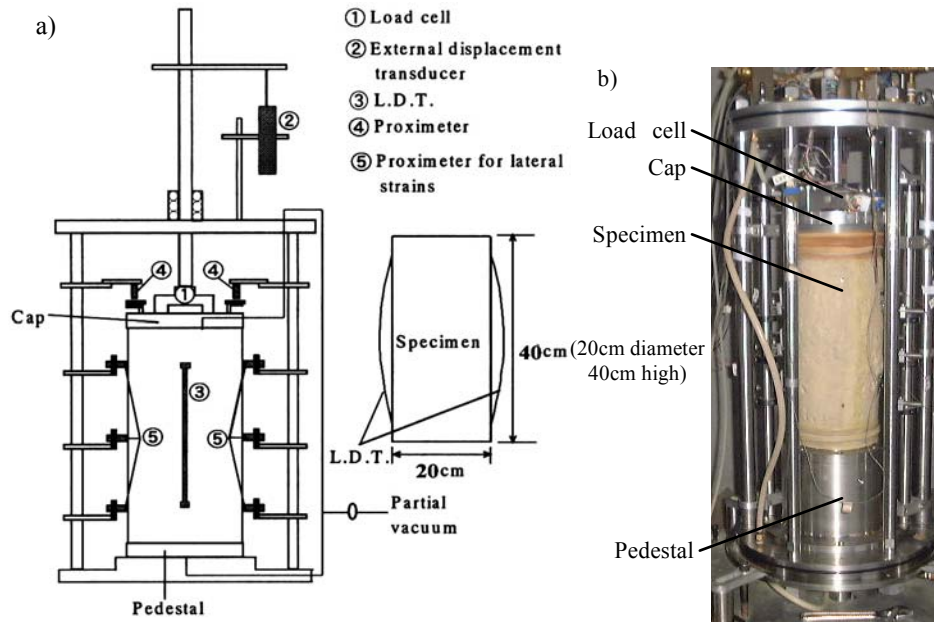


Fig. 15 Large triaxial apparatus; a) schematic diagram; and b) picture of the system during a TC test on cement-mixed Chiba gravel (Watanabe et al., 2003a).

3.3 Test results and discussions

Strength characteristic at different compacted dry densities. Figures 16a, b and c show typical results from CD TC tests on cement-mixed Chiba gravel specimens compacted to different dry densities, ρ_d , at a water content of 5 %. It may be seen that, with the same cement content by weight $W_{cement}/W_{gravel} = 2.5$ %, the peak strength increases significantly with an increase in the compacted dry density, ρ_d . On the other hand, the effects of ρ_d on the residual strength, defined at an axial strain of 15 %, are insignificant. It should be noted, however, the effects of ρ_d on the residual strength are not negligible, which is discussed below. Figures 17 and 18 summarise the peak and residual strengths plotted against the ρ_d value of solid material (gravel and cement).

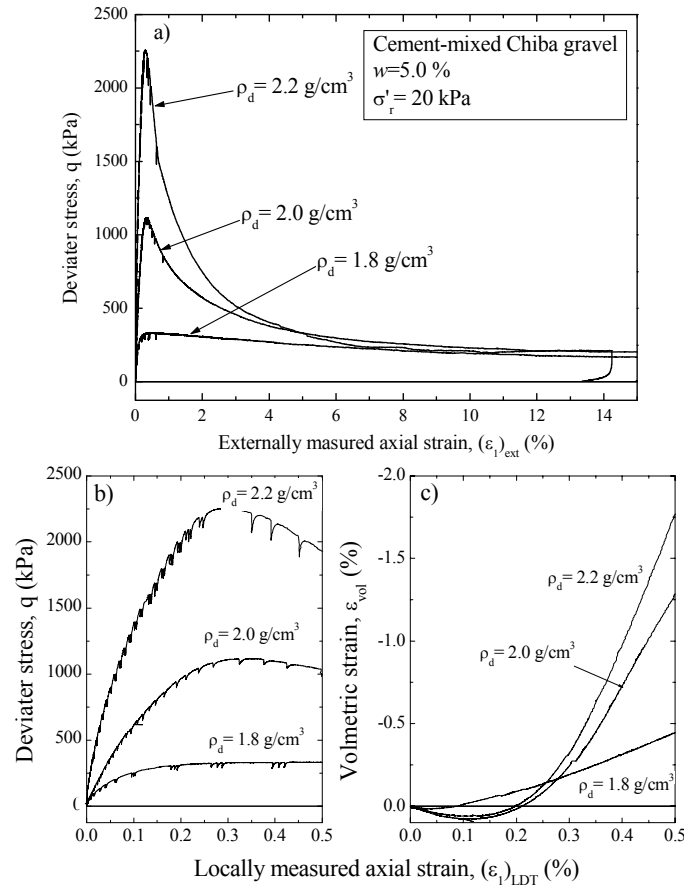


Fig. 16 a) Overall deviator stress-axial strain (external) relations; b) deviator-axial strain (local) relations at small strains; and c) volumetric and axial strain relations at small strains, cement-mixed Chiba gravel compacted different dry densities (Watanabe et al., 2003a).

The following trends of behaviour may be seen from these figures:

1. With both types of cement-mixed gravel, the peak strength increases with an increase in ρ_d at a rate that is much larger than with the uncemented ones. Therefore, the difference in the peak strength between the cement-mixed and uncemented specimens increases with an increase in ρ_d , in particular with Kyushu gravel.
2. When compacted by using nearly the same energy and with the same cement/gravel ratio by weight (W_{cement}/W_{gravel}), the peak strength of cement-mixed Kyushu gravel is significantly larger than that of cement-mixed Chiba gravel. This feature is discussed in detail later.
3. The effects of ρ_d on the residual strength are much smaller than the peak strength. Careful observations of the specimens of cement-mixed

gravel after the respective TC test indicated that the residual strength was controlled by frictional resistance along a shear band(s), not by bonding at inter-particle contacts along the shear plane.

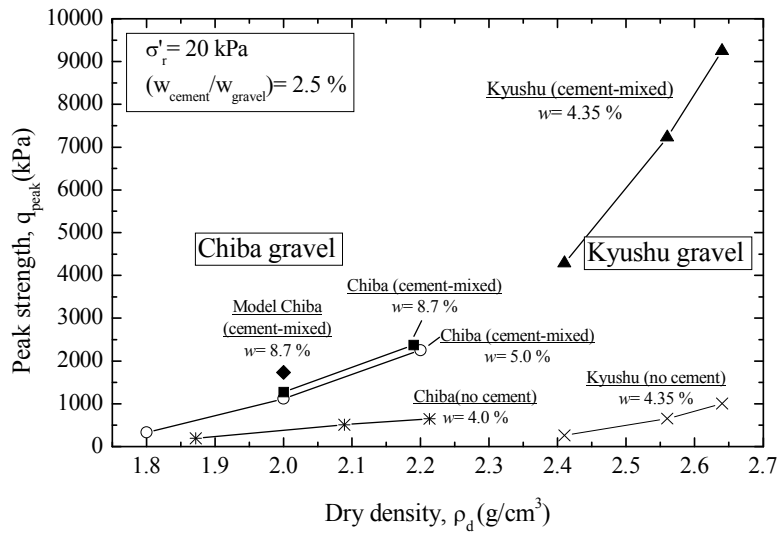


Fig. 17 Relationships between peak strength and compacted dry density of cement-mixed gravels and uncemented gravels (Watanabe et al., 2003a).

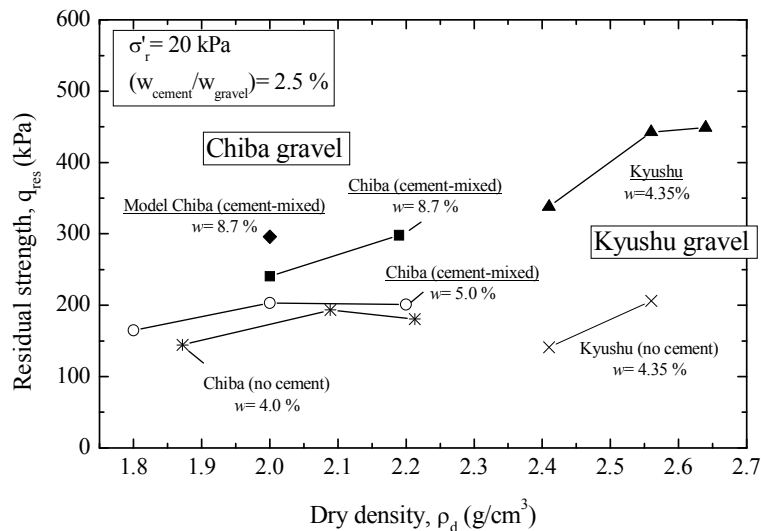


Fig. 18 Relationships between residual strength and compacted dry density of cement-mixed gravels and uncemented gravels (Watanabe et al., 2003a).

4. For the same ρ_d value, the peak strength of the cement-mixed specimen of the model Chiba gravel, not including particles larger than 10

mm and having a smaller coefficient of uniformity, is noticeably larger than that of cement-mixed original Chiba gravel. On the other hand, it is shown in Lohani et al. (2004) and Kongsukprasert et al. (2005) that, when compacted by using the same energy, the strengths of the cement-mixed model Chiba gravel and the original type of Chiba gravel with the same cement/gravel ratio by weight are nearly the same. These trends of behaviour are consistent with each other, because, for the same compaction energy, the ρ_d value is larger with the original Chiba gravel than the model Chiba gravel.

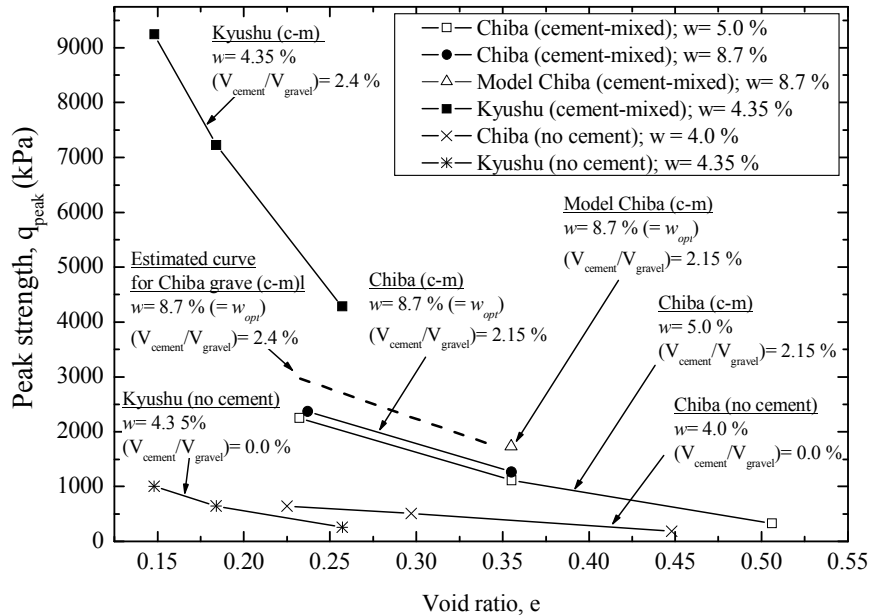


Fig. 19 Relationships between peak strength and compacted void ratio of cement-mixed gravels and uncemented gravels (Watanabe et al., 2003a).

The strength of cement-mixed Kyushu gravel is considerably higher than cement-mixed Chiba gravel for the same cement/gravel content by weight and for the same compaction energy. This trend of behaviour could be attributed to several factors. Firstly, a considerably higher ρ_d value for the same compacted void ratios (as shown in Figure 19) of Kyushu gravel can be attributed to a specific gravity of soil particles ($G_s = 3.03$) that is much larger than 2.71 of Chiba gravel. For the same cement/gravel ratio by weight, $W_{cement}/W_{gravel} = 2.5\%$, the cement content ($W_{cement}/\text{specimen volume } V'$) is proportional to ρ_d . Therefore, for the $q_{peak} - \rho_d$ relation for the same type of gravel plotted in Figure 17, two

variables, compacted dry density $\rho_d (= (W_{gravel} + W_{cement})/V)$ and cement content per volume ($= W_{cement}/V$), change simultaneously. It is likely, on the other hand, that the specific gravity of soil particles itself has no direct link to the packing conditions of particles, and, therefore, the peak strength of cement-mixed gravel is better linked to volume parameters than mass parameters, i.e., the void ratio ($= V/(V_{gravel} + V_{cement}) - 1.0$) rather than the ρ_d value and V_{cement}/V than W_{cement}/W_{gravel} . Then, when the peak strengths of cement-mixed Chiba and Kyushu gravels are compared for the same void ratio, the following two factors should also be considered.

- 1) For the same W_{cement}/W_{gravel} ($= 2.5\%$) and the same void ratio of solid part, the cement/gravel ratio in volume (V_{cement}/V_{gravel}) is different, equal to 2.4% with Kyushu gravel and 2.15% with Chiba gravel.
- 2) The ratios of the moulding water content (4.35% with cement-mixed Kyushu gravel and 8.7% with cement-mixed Chiba gravel) to the respective optimum water content are different. It is shown in Lohani et al. (2004) and Kongsukprasert et al. (2005), for the same type of cement-mixed gravel, even at the same compacted dry density, the peak strength becomes largest when compacted at the optimum water content (w_{opt}). Although it is subtle, this trend of behaviour can be seen by comparing the peak strengths of cement-mixed Chiba gravel specimens compacted at water contents of 5% (dry of optimum) and 8.7% (at optimum) in Figures 17 and 19.

In Figure 19, the strength curve for $V_{cement}/V_{gravel} = 2.4\%$ of cement-mixed Chiba gravel and the moulding water content equal to the optimum, which was estimated based on the results from a study on the effects of cement content and water content on the peak strength (Lohani et al., 2004; Kongsukprasert et al., 2005), is also presented. When compared at the same V_{cement}/V_{gravel} ($= 2.4\%$) and the same water content ratio $w/w_{opt} = 1.0$, the difference in the peak strength between the two types of cement-mixed gravel at the same void ratio becomes noticeably smaller than when compared at the same W_{cement}/W_{gravel} ($= 2.5\%$) and at the different moulding water content ratios, w/w_{opt} . Yet, the peak strength of cement-mixed Kyushu gravel is still noticeably larger than the cement-mixed Chiba gravel in Figure 19. Another factor (or others) is (are) necessary to explain this difference. The grading characteristics may be one of these factors.

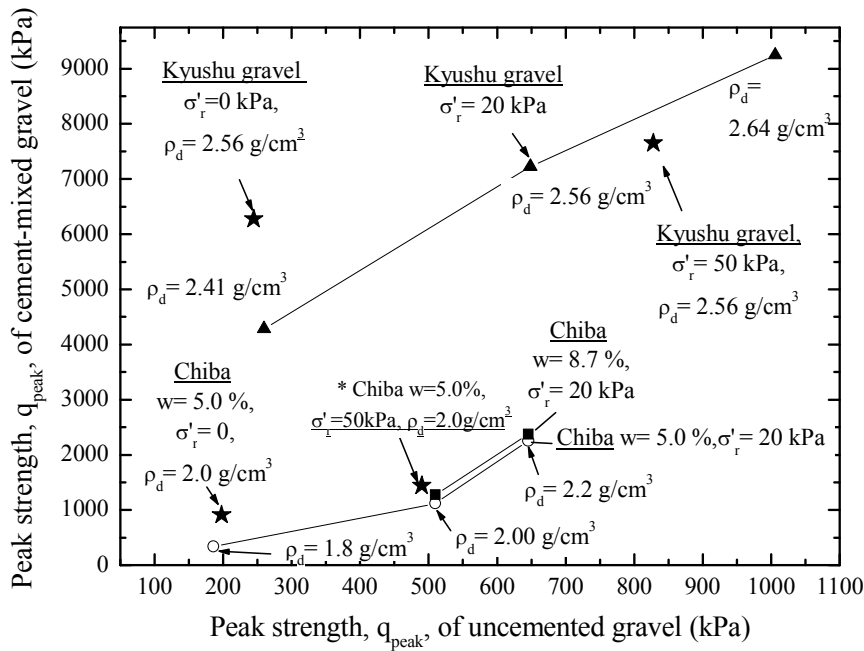


Fig. 20 Relationship between peak strengths of cement-mixed gravel and uncemented gravel; the water contents shown in this figure are for cement-mixed specimens (Watanabe et al., 2003a).

Figure 20 shows the relationships between the peak strengths of cement-mixed gravel and corresponding uncemented original gravel measured at the same confining pressure, $\sigma'_c =$ either 0 or 20 kPa or 50 kPa. The peak strength of uncemented Chiba gravel at $\sigma'_c = 50$ kPa was estimated from those extrapolated from the $q_{\text{peak}} - \sigma'_c$ relation obtained by CD TC tests performed at other similar σ'_c values. The following trends of behaviour may be seen:

1. The peak strengths of cemented and uncemented specimens compacted to the same dry density are well correlated to each other. This fact indicates the importance of increasing as much as possible the compacted dry density when the backfill is constructed by using cement-mixed gravel, in the same way with unbound original gravel.
2. The relationship between the peak strengths of cemented and uncemented specimens is not unique, affected by several other factors, including cement content, moulding water content, gravel type and confining pressure. The ratio of the peak strengths of cement-mixed gravel and uncemented gravel increases with a decrease in σ'_c .

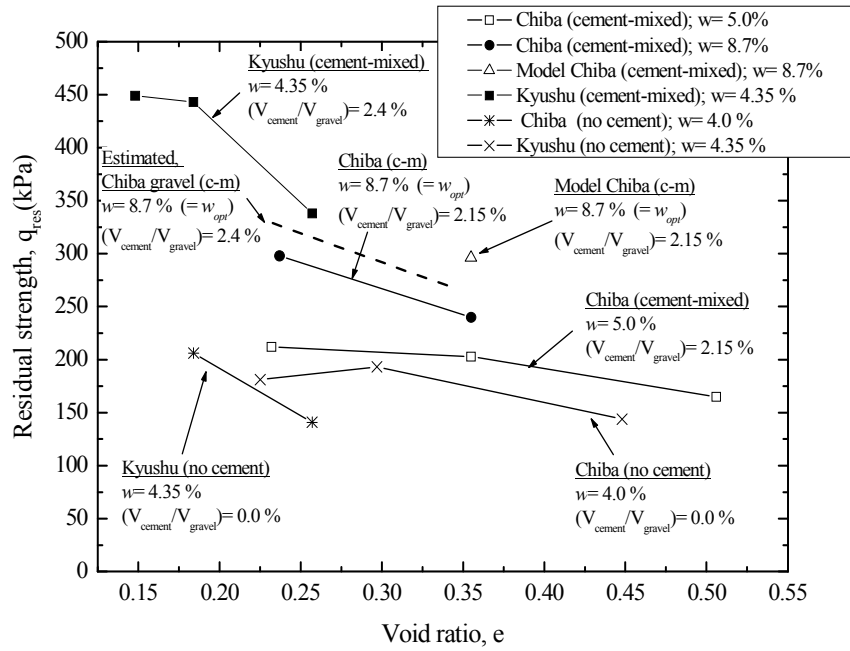


Fig. 21 Relationships between residual strength and void ratio of cement-mixed gravels and uncemented gravels (Watanabe et al., 2003a).

Figure 21 compares the residual strength in the same way as Figure 19. Also in this figure, the estimated strength curve for $V_{cement}/V_{gravel}=2.4\%$ of cement-mixed Chiba gravel compacted at the optimum water content is presented. Although they are much less pronounced, the trends of behaviour that can be seen with the peak strength in Figure 19 can also be seen in this figure, indicating that the peak and residual strengths are linked to each other. Figure 22 shows the relationships between the corresponding peak and residual strengths of uncemented and cement-mixed specimens of Chiba and Kyushu gravels. It may be seen that the residual strength becomes larger with an increase in the peak strength in a similar way irrespectively of gravel type and whether the specimen is uncemented or cement-mixed. That is, the residual strength of cement-mixed gravel is noticeably larger than that of the corresponding uncemented gravel. It seems that the residual strength of cement-mixed gravel is controlled by not only the friction at inter-particle contacts but also restraining from free rotation of soil particles by bonding at inter-particle contacts; that is, the roughness along a shear plane increases with an increase in the inter-particle bond strength.

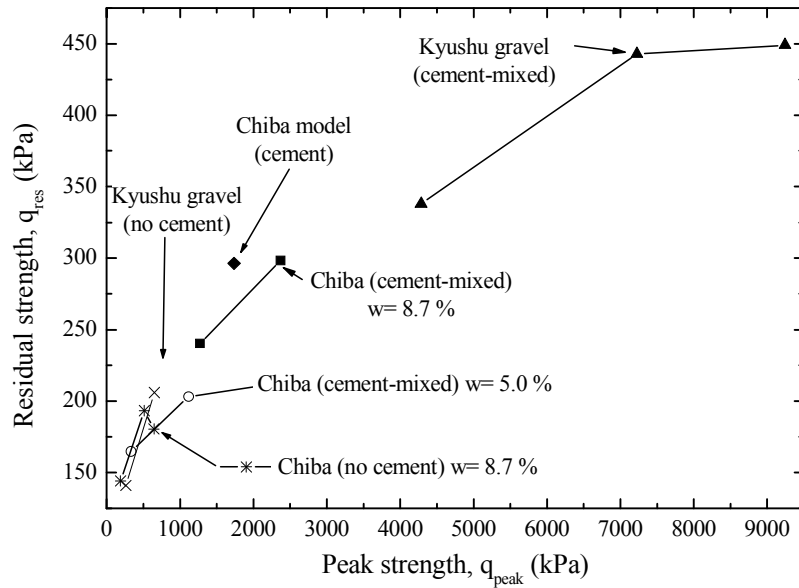


Fig. 22 Relationship between residual strength and peak strengths of cement-mixed gravel and uncemented gravels (Watanabe et al., 2003a).

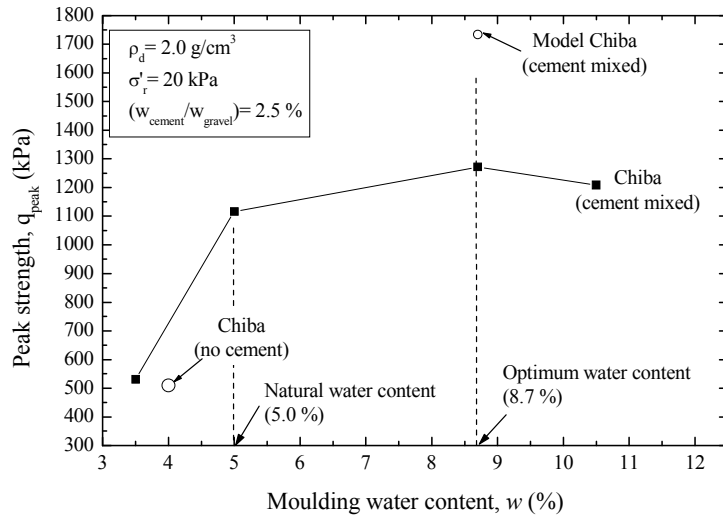


Fig. 23 Relationship between peak strength and moulding water content (Watanabe et al., 2003a).

Effects of moulding water content. Figure 23 shows the relationships between the peak strength and the moulding water content for cement-mixed Chiba gravel. It may be seen that the peak strength became the maximum around the optimum water content ($w_{opt} = 8.7\%$). This trend of behaviour is due mostly to the largest compacted dry density (i.e., the

smallest compacted void ratio). The other influencing factors include; a) the largest cement content per volume of specimen associated with the maximum compacted dry density (as discussed above); and b) the optimum cement paste conditions in terms of the volume of paste and the strength of paste (Lohani et al., 2003 & 2004; Kongsukprasert et al., 2005; and as discussed below). With respect to the term b), the strength of cement paste decreases with an increase in the moulding water content examined in the present study. It is likely that the decrease in the strength of cement-mixed gravel with an increase in the water content larger than w_{opt} is due to this factor. On the other hand, the amount of cement paste decreases with a decrease in the moulding water content. In fact, the peak strength when compacted at $w= 3.5\%$ is very small, close to the peak strength of uncemented gravel. It appears that this very low strength was due to an insufficient amount of cement paste to be distributed uniformly at inter-particle contacts. It is shown in Lohani et al. (2004) and Kongsukprasert et al. (2005) that the same trends of behaviour were also observed in the TC tests on small specimens of cement-mixed model Chiba gravel. These results indicate that the water content should be controlled as strictly as possible, preferably at the optimum water content, when compacting a given type of cement-mixed gravel in actual construction projects.

Table 3 Internal friction angles and cohesion intersects of cement-mixed and uncemented gravels (Watanabe et al., 2003a).

Gravel type	Peak		Residual	
	ϕ_{peak} (deg.)	c_{peak} (kPa)	ϕ_{res} (deg.)	c_{res} (kPa)
Chiba gravel (cement mixed)	57.4	132	55.9	0
Chiba gravel (no cement)	48.9	38.4	48.9	0
Kyushu gravel (cement mixed)	68.4	614	61.8	0
Kyushu gravel (no cement)	58.1	44.7	49.2	0

Mohr-Coulomb strength parameters: Figure 24 shows the peak and residual strengths plotted against the effective confining pressure, σ'_c , for the cement-mixed gravel specimens with $W_{cement}/W_{gravel} = 2.5\%$ and the corresponding uncemented gravel specimens. The water content was equal to the optimum water content for Kyushu gravel, while it was 5.0 % for cemented Chiba gravel and 4.0 % for uncemented Chiba gravel. Table 3 shows the angle of internal friction and cohesion intersect of the

respective type of specimen obtained from the failure envelopes presented in Figure 24. The residual strength in the unconfined compression tests on cemented and uncemented specimens was equal to zero (i.e., $c_{res} = 0$).

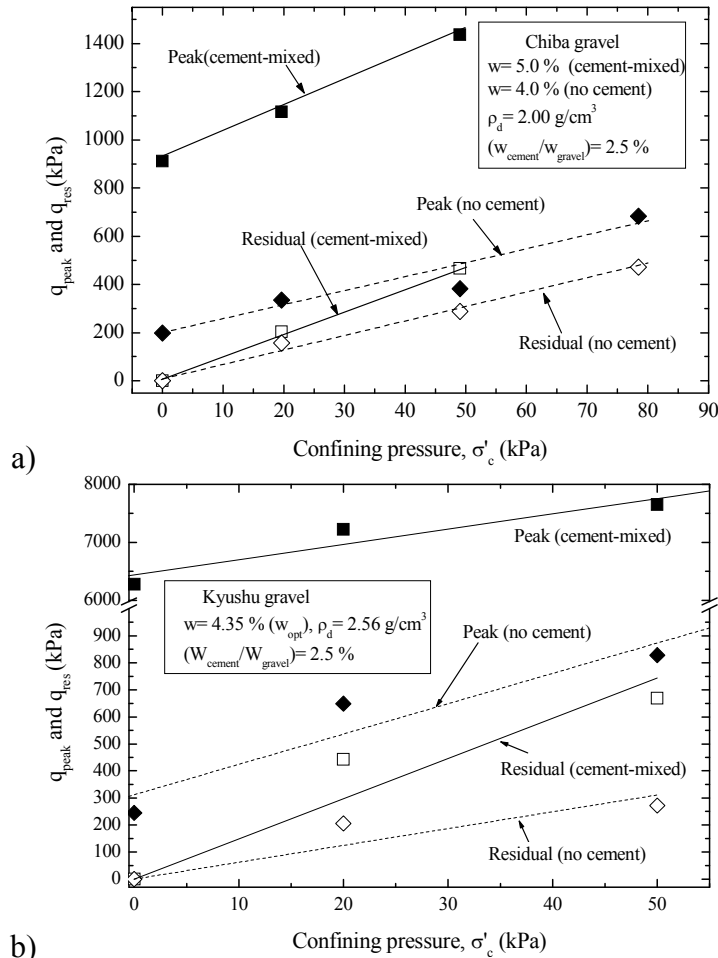


Fig. 24 Relationships between peak and residual strengths and confining pressure; cemented and uncemented specimens of a) Chiba gravel; and b) Kyushu gravel (Watanabe et al., 2003a).

The following trends of behaviour may be seen from Figure 24 and Table 3:

- 1) Not only the cohesion intercept, c_{peak} , but also the angle of internal friction, ϕ_{peak} , increase considerably by cement-mixing. This trend of behaviour is in contrast to the case with cement-mixed soft clay, for

which the φ_{peak} value largely decreases while the c_{peak} value largely increases by cement-mixing (as reported by Tatsuoka et al., 1997a; Sugai et al., 2000 & 2003). It is likely that the large peak strength of cement-mixed gravel results from restraint to not only sliding but also rotation of soil particles by bonding at inter-particle contacts. Note that the effects of the increase in c_{peak} on the shear strength are significant at low σ_c' values.

- 2) The φ_{peak} values of both cement-mixed and uncemented specimens of Kyushu gravel are considerably larger than the respective value of cement-mixed and uncemented specimens of Chiba gravel. The increase in c_{peak} by cement-mixing is much larger with Kyushu gravel than with Chiba gravel. It is not well understood how this feature can be linked to the gravel type, such as fines content, particle shape, grading characteristics, the mother rock type and so on.

The use of these peak strength parameters in the limit-equilibrium type stability analysis may result in an over-estimation of safety factor because of possible large effects of progressive failure (Tatsuoka et al., 2000). The use of values between the peak and residual strengths would be relevant. Further study is necessary in this respect.

3.4 Summary of CD TC test results

The following conclusions can be derived from the results for the CD TC tests on large specimens of cement-mixed gravel presented above:

1. The peak strength of compacted cement-mixed gravel could become significantly larger than that of uncemented gravel. The difference increases with an increase in the compacted dry density. This result indicates the significant importance of compaction control when constructing the backfill of cement-mixed gravel as with the backfill of uncemented gravel.
2. For different types of gravelly soil having different specific gravities of particles, the strength of cement-mixed gravel should be considered as a function of compacted void ratio, rather than dry density, as well as cement/gravel ratio by volume rather than cement/gravel content by weight. The gravel type is another important influencing factor.
3. The strength of cement-mixed gravel becomes the maximum at the optimum water content, which could be due not only to the maximum compacted dry density (or the minimum compacted void ratio) and the associated maximum cement content per volume of specimen but also to the optimum cement paste conditions in terms of volume and strength. In fact, the strength when compacted significantly drier of

optimum could be very small, perhaps due to an insufficient distribution of cement paste at inter-particle contacts.

4. Not only the cohesion intercept but also the angle of internal friction could significantly increase by cement-mixing, unlike cement-mixed clay. The contribution of cohesion intercept to the shear strength becomes particularly large at low effective confining pressures.
5. Despite that the increase is much smaller than that of the peak friction angle by cement-mixing, the friction angle at the residual state could noticeably increase by cement-mixing. With cement-mixed gravel, the residual strength is well correlated to the peak strength.

4. CONSTRUCTION OF A PROTOTYPE NEW TYPE RIDGE ABUTMENT

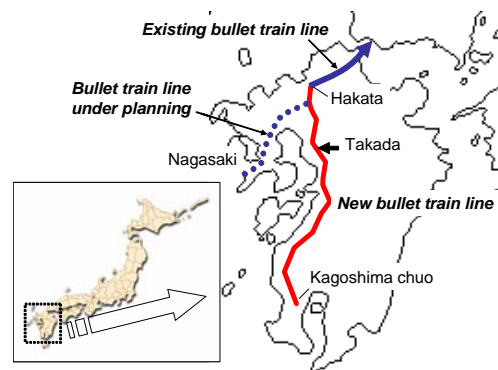


Fig. 25 Location of the new type bridge abutment using cement-mixed gravel at Takada, Kyushu (Aoki et al., 2002).

4.1 Introduction

Based on the results from the laboratory stress-strain tests on cement-mixed gravel described in the preceding sections, in 2002, the Japan Railway Construction Public Cooperation started the design of a new type bridge abutment to be constructed at Takada, Kyushu, for a new bullet train line, considering cost-effectiveness (Figure 25) (Aoki et al., 2002). Figure 26a shows the outline of the bridge abutment and Figure 26b shows a view of the completed abutment. The construction started November 2002 and ended two months later. To confirm whether the vertical bearing capacity and the lateral stability of the parapet structure (RC parapet) of the abutment are sufficiently high, which is the most cru-

cial feature of the new structural type of bridge abutment, full-scale field loading tests were performed in the last week of February 2003. The results were very satisfactory as shown below.

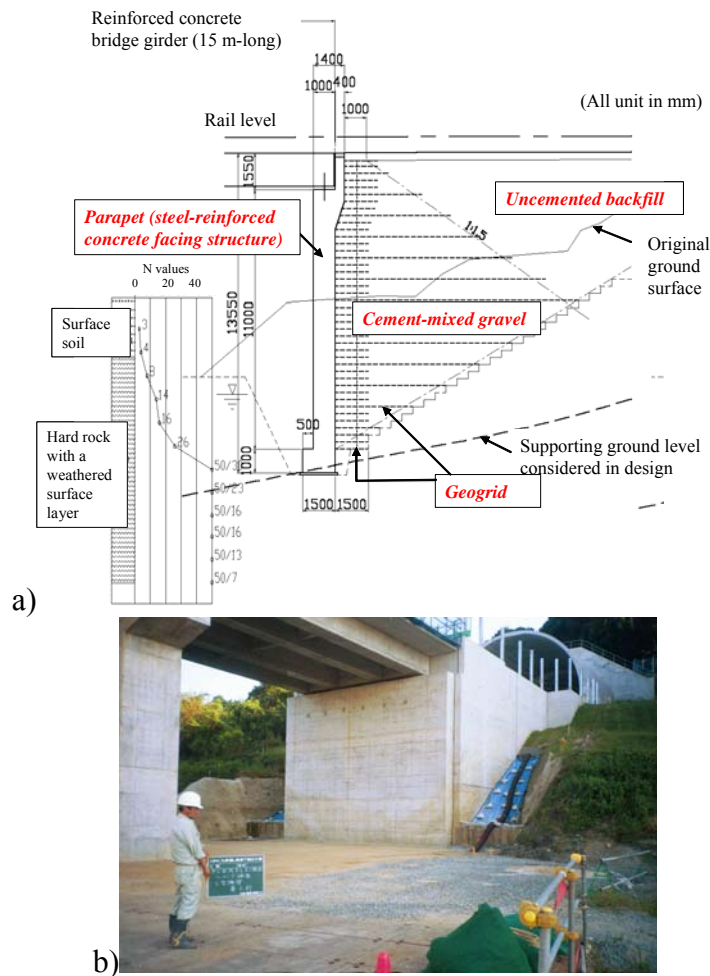


Fig. 26 a) New type bridge abutment using cement-mixed gravel constructed at Takada (Aoki et al., 2002); and b) view of the completed new type bridge abutment, mid 2003.

4.2 Design

For the new bullet train line, the design train speed is 260 km/h and the standard design train load (live) load is P-16. That is, 16 tonf or 157 kN is applied to one axle having two wheels. Each pair of axles with a minimum center-to-center distance of 2.2 m supports one bogie, while two bogies with a center-to-center distance of 15 m support one 20 m-long

coach. The abutment supports a simple beam T-shaped RC girder having a length of 15 m with a fixed end at the top of the parapet. It was decided that the design compressive strength of cement-mixed backfill is 2 MPa and the design rupture strength of geogrid is 30 kN/m. The soil layers having blow counts (N values) by the standard penetration tests equal to or larger than 50 were considered as the supporting ground of the RC parapet, while the soil layers having N values equal to or larger than 9 were considered as the supporting ground of the approach block (i.e., backfill of cement-mixed gravelly soil).

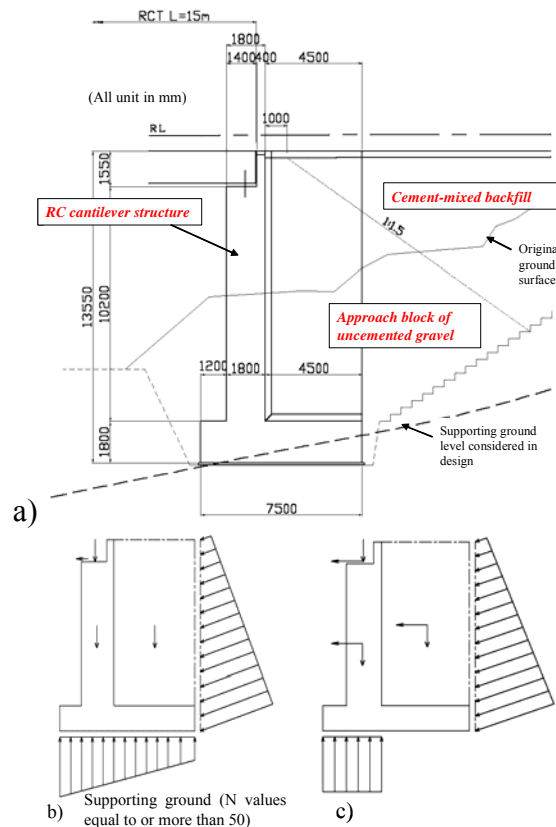


Fig. 27 a) Conventional type bridge abutment: b) static and c) seismic loading conditions for conventional type bridge abutment (Aoki et al., 2002).

Figure 27a shows the conventional type bridge abutment that would have been constructed if the new structural type one (Figure 26) had not been adopted. The RC conventional type bridge abutment was designed as a cantilever structure resisting against the static earth pressure exerted by the uncemented backfill as well as the static load of the RC abutment

and bridge girder and the live load under static loading conditions (Figure 27b). For seismic design, the dynamic component of earth pressure and the inertia of the RC abutment and bridge girder should be additionally taken into account (Figure 27c).

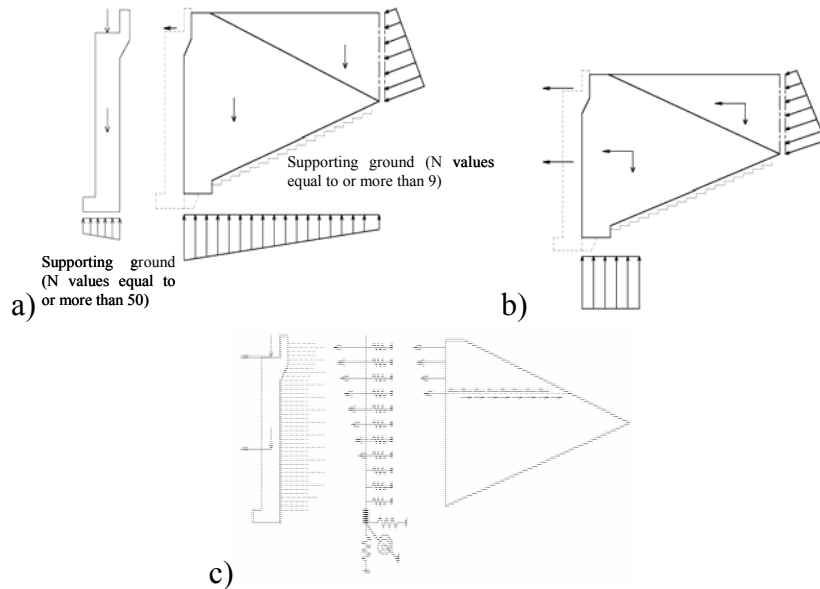


Fig. 28 a) Static; and b) seismic loading conditions; and c) seismic conditions at the connection, for new type bridge abutment (Aoki et al., 2002).

With the new type abutment, the RC parapet and the backfill of cement-mixed gravelly soil were designed as separate structural components (Figures 28a & b). The RC parapet was designed to support the static and dynamic loads of the parapet and those from the bridge girder with the live load. The static and dynamic earth pressures from the backfill were not taken into account considering that the lateral outward movement of the parapet should be supported by the cement-mixed backfill under seismic loading conditions. Therefore, the tensile strength of the geogrid layers that connect the parapet and the backfill should be sufficiently high to withstand the tensile load activated by the outward lateral movement of the parapet during seismic loading conditions. As shown in Figure 28c, the distribution of tensile force at the connections was obtained by modeling the connections by a series of spring. The backfill of cement-mixed gravelly soil was designed as a gravity-type earth retaining wall resisting the lateral load from the parapet and the earth pressure from the unbound soil backfill in back of the cement-mixed gravel back-

fill. Several long layers of geogrid were arranged at a vertical spacing of 0.9 m, prepared for possible development of tension cracks during severe seismic loading conditions. The strength of the long layers was determined to resist the seismic tensile force acting at the vertical plane at the back end of the short layers ignoring the tensile strength of the backfill. The tensile force was obtained by assuming the zone in front of this vertical plane to act as a monolith.

The construction cost of the new type bridge abutment was estimated to be 87 % of the conventional type for good ground conditions at the site. If the ground condition were poorer and the conventional type bridge abutment should have been supported by a pile foundation (as in many cases), as the new type one needs not a pile foundation, the difference in the construction cost could become much larger than the present case.

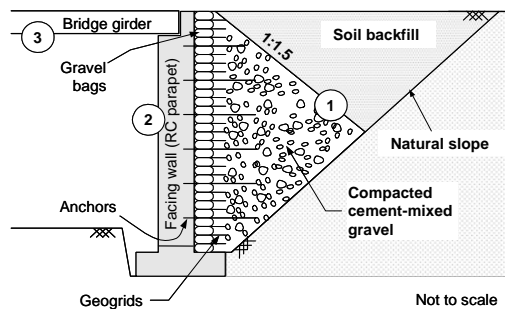


Fig. 29 Staged construction method for new type bridge abutments with backfill of cement-mixed gravel (Watanabe et al., 2003b; Aoki et al., 2003)



Fig. 30 Compaction of the backfill

4.3 Construction

The abutment was constructed by the staged construction method (Figure 29). That is, the backfill was constructed before constructing the RC

parapet. A well-graded crushed gravelly soil of gabbro from a quarry (classified as M-40; typically, $D_{\max} = 37.5$ mm, $D_{50} = 5.4$ mm, $U_c = 61$, a fines content = 6 %, and a specific gravity = 3.03) was used as the backfill. The stress-strain properties of cement-mixed specimens of this type of gravel were described in the preceding section. The maximum compacted dry density, $(\rho_d)_{\max}$, was 2.60 g/cm^3 at the optimum water content, $w_{\text{opt}} = 4.9 \%$ by the compaction tests using a mould with an inner diameter of 15 cm and an inner height of 12.5 cm with an energy level of 2480 kJ/m^3 (the $E-b$ method, the Japanese Industrial Standards A1210 (Watanabe et al., 2003b)). The lift of compacted soil layer was made as small as 15 cm to obtain a high compacted dry density. The specified compaction energy was achieved by ten times passing of a small vibratory compaction plant with a weight of about 1 tonf for the first 24 lifts (Figure 30a) while six times passing of a vibratory plant with a weight of about 4 tonf for the 25th through 81st lifts (Figure 30b). A cement-mixed ratio by weight equal to 4 % was employed. This ratio, which was higher than the value used in the laboratory stress-strain tests, was employed by taking into account a possibly high degree of inhomogeneity of cement mixing in the field.

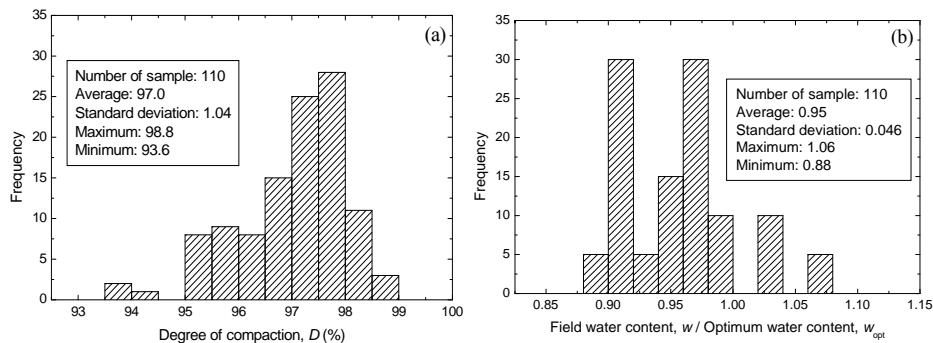


Fig. 31 a) Degree of compaction; and b) water content measured during the construction of backfill (Watanabe et al., 2003b).

The field compaction was made with a lift of 15 cm so as to obtain a degree of compaction more than 95 %. Figures 31a and 31b show the frequency distributions of compacted dry density (by means of RI) and water content measured during the construction. It may be seen that the results were satisfactory. The compaction of the backfill in the field was made with a help of bags filled with unbound gravel placed at the shoulder of each soil layer (Figure 32a).



Fig. 32 a) Placing gravel-filled bags at the shoulder of each soil layer; steel reinforcement seen in this picture is for the parapet that was constructed after the backfill was completed (Watanabe et al., 2003b); and b) bridge abutment with backfill of cement-mixed gravel during full-scale loading test.

As the bags were wrapped around with polymer geogrid layers, the wall face of the completed backfill was covered with geogrid sheets. The RC parapet was constructed by casting-in-place fresh concrete into a space between an external concrete form supported by steel bars extending from the inside of the backfill and the wall face of the backfill (Figure 32a). Steel reinforcement had been arranged in the space. Therefore, the parapet had been firmly connected to the geogrid sheets and gravel bags when the parapet was completed. By this staged construction method, the following potential problems in case the RC parapet were constructed prior to the construction of backfill can be avoided:

- 1) If the parapet is first constructed, too large earth pressure may be exerted on the parapet during compaction of backfill. To avoid this problem, the zone of backfill adjacent to the back face of the parapet may not be well compacted, forming a structurally weak zone.
- 2) If the reinforcement layers are connected to the back face of the parapet during the construction of the backfill, the connection could be damaged in case the settlement of the backfill relative to the parapet during the construction of the backfill becomes too large.
- 3) To keep the alignment of the front face of the parapet as constructed, the parapet should be supported with a very stiff propping during the construction of the backfill. Otherwise, the footing of the parapet should be made wider while supported with a pile foundation.

Figure 32b shows the bridge abutment with the completed parapet during the full-scale loading test described below.

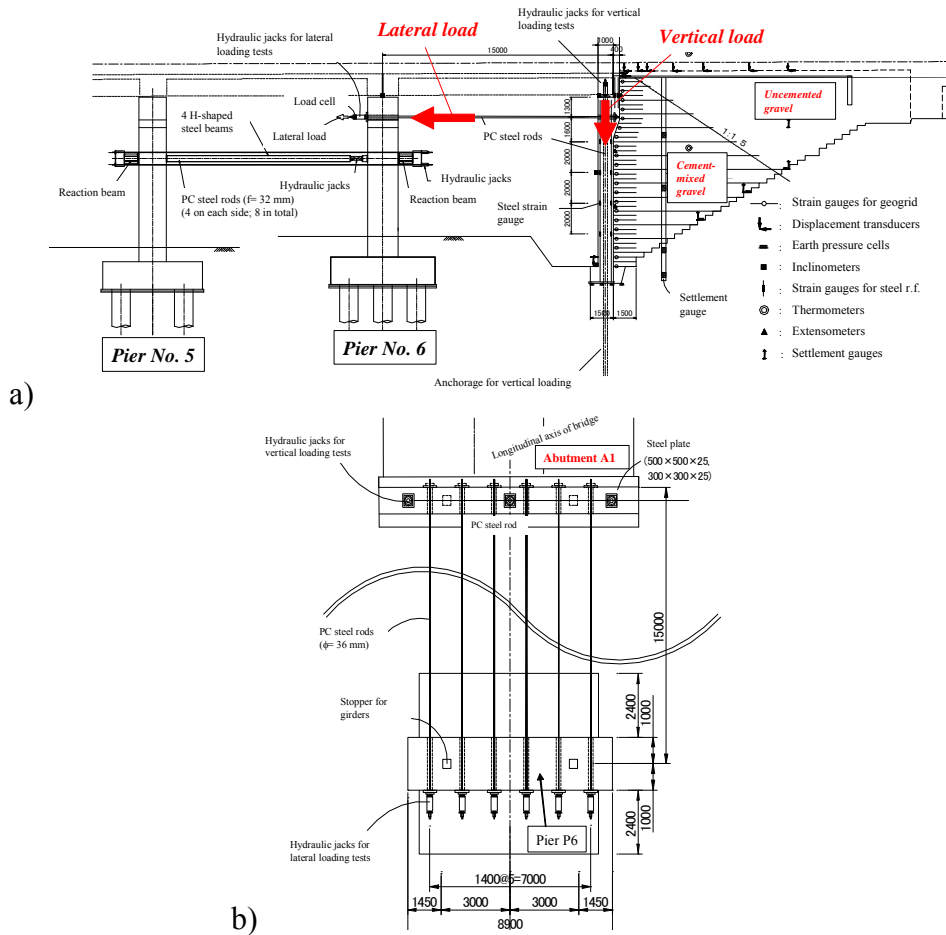


Fig. 33 a) Profile; and b) plan of field full-scale loading test of the bridge abutment with backfill of cement-mixed gravel (Aoki et al., 2003).

4.4 Full-scale loading tests

To confirm whether the new type abutment is sufficiently stable under severe seismic loading conditions as considered in the design, full-scale vertical and lateral loading tests were performed on the completed abutment (Aoki et al., 2003) (Figures 33a & 33b). First, vertical load **simulating the deadweight of bridge girder** was applied to the top of the RC parapet by means of three hydraulic jacks arranged at the shoulder of the parapet, which is the fixed end of a bridge girder, and PC steel rods (tendons) anchored into the supporting ground. Then, lateral load was applied to the parapet at 1.3 m below the shoulder by using six hydraulic jacks arranged at the adjacent pier. Two piers Nos. 5 and 6 were fixed to each other to react as a unit against the lateral load (Figure 34), because it

was anticipated that the abutment would be much stronger against lateral loading than a single pier. It was confirmed that, despite relatively small dimensions of the footing for the parapet, the vertical bearing capacity of the footing is sufficiently large as anticipated. In the following, the results from the lateral loading tests are reported.

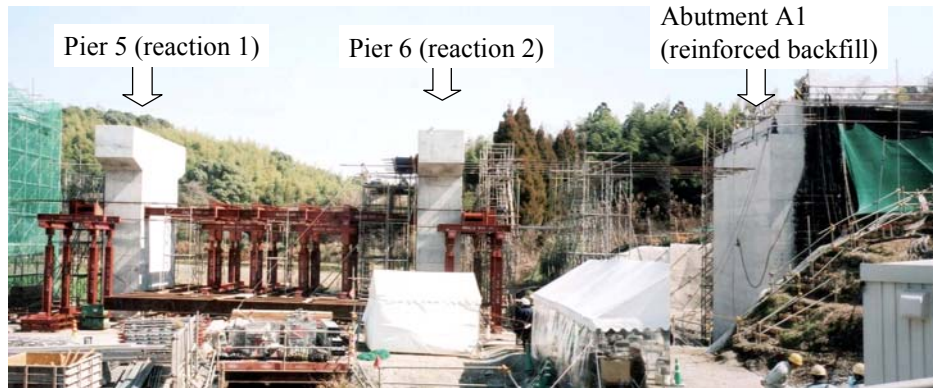


Fig. 34 Overview of field full-scale loading test of bridge abutment with backfill of cement-mixed gravel (Aoki et al., 2003).

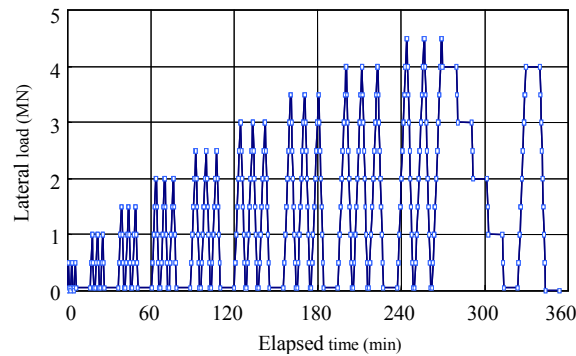


Fig. 35 Time history of lateral load applied to bridge abutment with backfill of cement-mixed gravel (Aoki et al., 2003).

Figure 35 shows the time history of lateral load. Figure 36a shows the relationship between the lateral load and the outward lateral displacement at the top of the parapet. Figure 36b shows the locations of lateral load application and measurement of several quantities. The lateral displacement at 1.3 m below the shoulder of the parapet at the maximum load (4 MN) was as small as 15.6 mm. A lateral load of 4 MN is only slightly lower than the design seismic lateral load, equal to 4.171 MN, for a design lateral seismic coefficient of as high as 0.89 corresponding to the design maximum ground horizontal acceleration equal to 871 gals (i.e.,

so-called level II design seismic load). The residual lateral displacement was 9.3 mm, compared with the maximum value equal to 15.1 mm, which means that the behaviour was rather recoverable, showing that the load-displacement state at a horizontal load of 4 MN was far before ultimate failure.

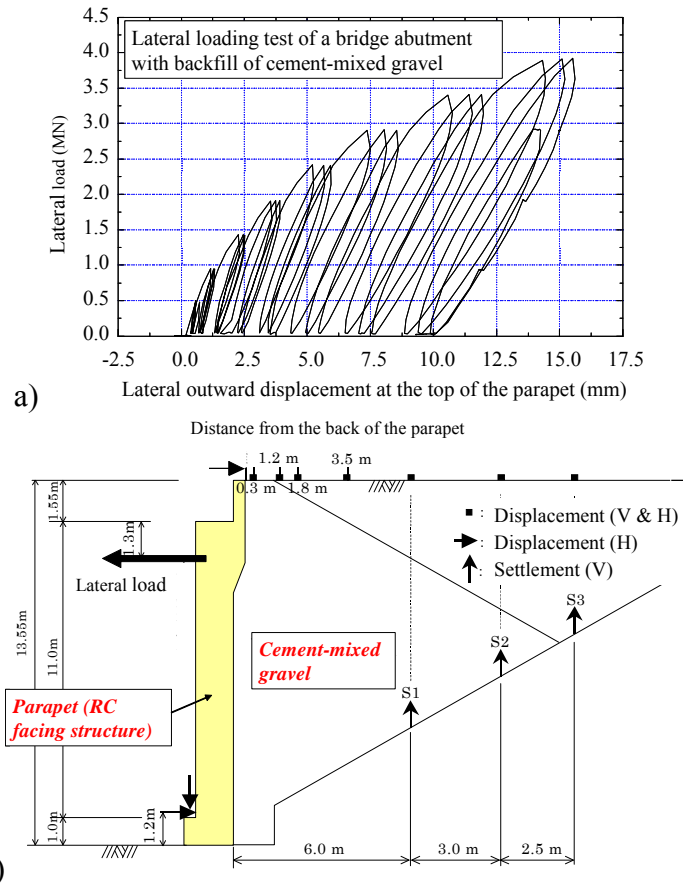


Fig. 36 a) Relationship between lateral load and lateral outward displacement at the top of the parapet; and b) locations of measurement, bridge abutment with backfill of cement-mixed gravel (Aoki et al., 2003).

Figures 37a, 37b and 37c show the vertical distributions of lateral displacement of the abutment and the adjacent two piers. The lateral displacements of the two piers was about two times as large as that of the abutment, which means that the lateral stiffness of the parapet is about four times as large as that of a single pier. This result indicates clearly

that this new type bridge abutment has a lateral stability much more than sufficient.

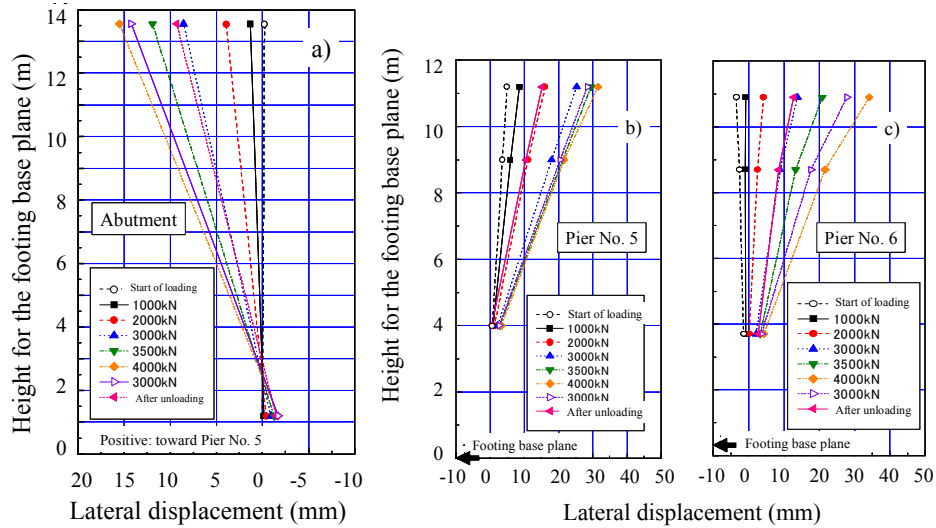


Fig. 37 Lateral displacements of a) abutment; b) pier No. 5; and c) pier No. 6 from lateral loading tests, bridge abutment with backfill of cement-mixed gravel (Aoki et al., 2003).

Figures 38a & 38b show the distributions of lateral displacement and settlement on the crest of the backfill from the back face of the parapet (see Figure 36b). Figure 38c shows the distribution of settlement at the base of the approach block and the distance from the back face of the parapet. The following trends of behaviour may be seen from these figures:

- 1) There was no distinct separation between the back of the parapet and the approach block, indicating that the geogrid did not show any large deformation at the connection.
- 2) The lateral displacement at the crest of the backfill was very uniform for a range of distance from zero to about 5.5 m, indicating that the approach block behaved like a monolith without developing major vertical cracks inside. A major crack with a width of about 10 mm was found at a distance of 7.25 m from the back face of the parapet at the end of loading (Figure 40).
- 3) The crest of the backfill exhibited noticeable settlements, which were larger at places closer to the parapet. This trend of behaviour was due mainly to a rigid overturning rotational displacement of the approach block, as shown below, caused by lateral loading.
- 4) The back zone of the approach block exhibited considerable heaving at the base associated with lateral loading (Figure 38c). Figure 39a

shows the changes in the earth pressure associated with lateral loading measured at the base of the approach block (see Figure 39b for the locations of the earth pressure cells). This result also indicates a rigid overturning rotational displacement of the approach block.

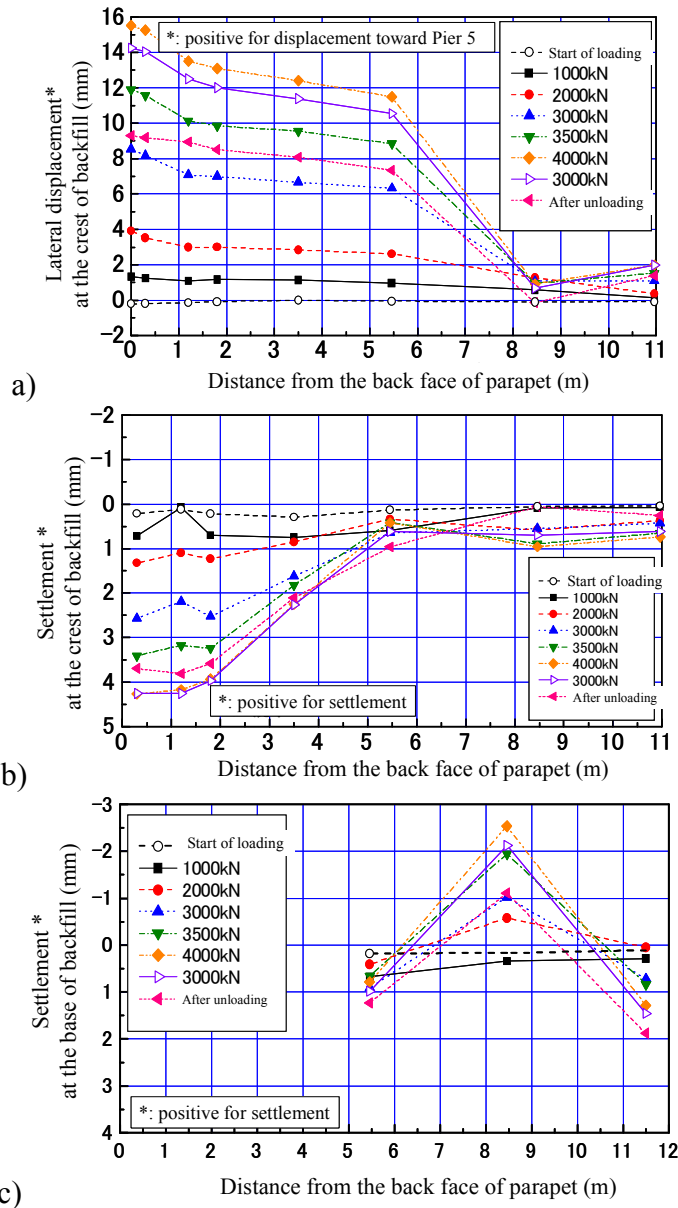


Fig. 38 a) Lateral displacements & b) settlement at the crest; and c) settlement at the base of backfill of cement-mixed gravel crest (Aoki et al., 2003).

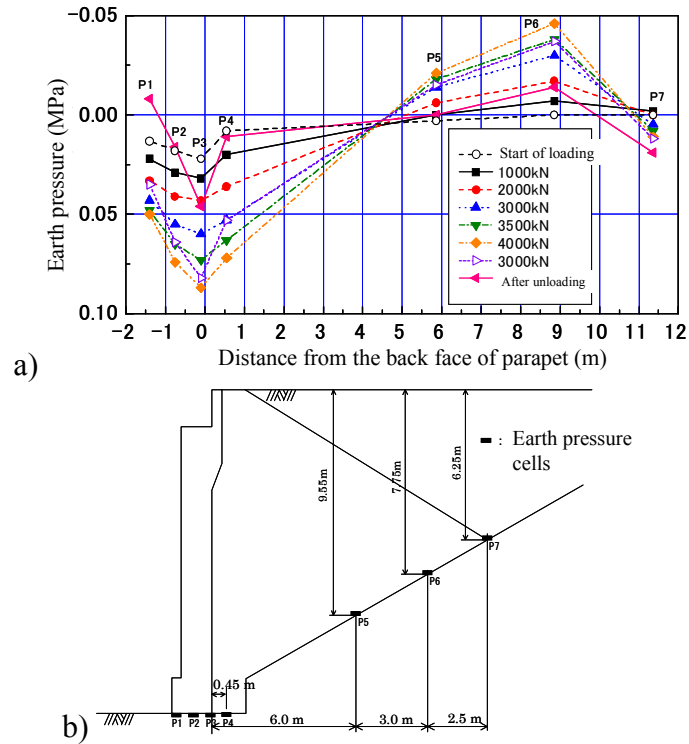


Fig. 39 a) Earth pressure at the base of backfill of cement-mixed gravel; and b) locations of earth pressure cells (Aoki et al., 2003).

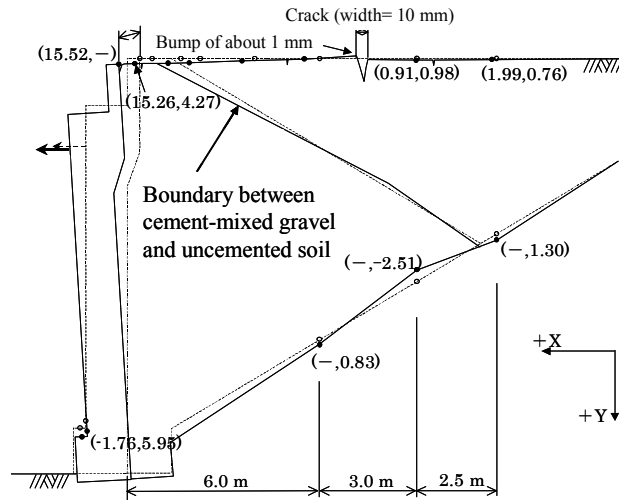


Fig. 40 Overall residual deformation observed at the maximum lateral load (Aoki et al., 2003)

Figure 40 shows the overall displacement of the abutment at the maximum lateral load. It may be seen that the parapet and the approach block of cement-mixed gravel behaved like a monolith exhibiting a rigid overturning rotational displacement, showing no sign of a separation between them, without development of major cracks inside the approach block.

4.5 Summary of results from a field full-scale loading test

The following conclusions can be derived from the test results presented above:

- 1) The new type bridge abutment has a lateral stiffness that is higher by a factor of about four than that of a single pier that was designed and constructed following the present seismic-resistant design code against severe design seismic load (so called level II).
- 2) The maximum and residual outward lateral displacements at the top of the parapet when subjected to a very high lateral load simulating severe design seismic load were as small as 15.6 mm and 9.3 mm, indicating a very high seismic stability of the new type bridge abutment.
- 3) Against very large lateral load, the parapet and backfill behaved like a monolith exhibiting a rigid overturning rotational displacement, showing no sign of a separation between them, without development of major cracks inside the approach block.

5. CONCLUDING REMARKS

Based on the results from the shaking table tests on scaled-models in the laboratory and the consolidated drained triaxial compression tests on cement-mixed gravel, a new structural type of bridge abutment was proposed. Subsequently, a prototype bridge abutment was designed and constructed. The advantages of the new type bridge abutment include a high cost-efficiency and a very high seismic stability without showing any serious bump immediately behind the back of front RC structure (i.e., parapet) supporting a bridge girder (or girders). The Japan Railway Construction Public Agency specified “Design and construction standard for bridge abutments having an approach block of cement-mixed backfill” March 2004 to construct new structural type bridge abutments at other places.

It is now possible to construct permanent civil engineering structures that need a high ultimate stability allowing relatively small displacements by constructing backfill of cement-mixed soil. This report describes a case history showing the above. In this case history, a proper understanding of the stress-strain properties (i.e., the strength and deformation characteristics) of cement-mixed soil was essential. To this end, systematic and careful laboratory stress-strain tests (mostly triaxial compression tests) were performed. The test results revealed that the stress-strain properties of different types of cement-mixed soil have common as well as specific features. The results from the laboratory stress-strain tests played major roles in the design.

ACKNOWLEDGEMENTS

The author expresses his sincere thanks to their past and present colleagues for their help in preparing this report; in particularly Prof. Koseki, J. of Institute of Industrial Science, University of Tokyo, Dr Lohani, T. N., Dr Kongsukprasert, L. and Dr Uchimura, T. for the report of the new type bridge abutment.

NOTATION

a_{\max} = amplitude of horizontal acceleration at the shaking table

c/g = cement-to-gravel ratio by weight

c_{peak} = cohesion intercept for peak strength

c_{res} = cohesion intercept for residual strength

D_{50} = mean diameter of particle

e = void ratio

q = deviator stress = $\sigma'_v - \sigma'_h$

q_{peak} = peak strength (compressive strength)

q_{res} = residual strength

w = water content

ε_v = axial strain

ϕ_{peak} = angle of internal friction for peak strength

ϕ_{res} = residual angle of friction for residual strength

ρ_d = dry density

REFERENCES

Aoki, H., Yonezawa, T., Hashimoto, J., Tateyama, M., Yamada, T., Kohara, A. and

- Tatsuoka, F. (2002). Comparative design of bridge abutment with backfill of cement-treated soil and conventional type abutment. *Proc. 37th Japan National Conf. on Geotech. Eng., Japanese Geotech. Society*, Osaka, pp. 805-806 (in Japanese).
- Aoki, H., Yonezawa, T., Watanabe, O., Tateyama, M. and Tatsuoka, F. (2003). Results from field full-scale loading tests on a bridge abutment with backfill of geogrid-reinforced cement-mixed gravel." *Geosynthetics Engineering Journal, Japanese Chapter of International Geosynthetics Society*, 18, 237-2428 (in Japanese).
- Goto, S, Tatsuoka, F., Shibuya, S., Kim, Y.-S., and Sato, T.(1991). A simple gauge for local small strain measurements in the laboratory. *Soils and Foundations*, Vol. 31, No. 1, pp. 169-180.
- Hansen, K. D. and Reinhardt, W.G. (1990). *Roller-compacted concrete dams*" McGraw-Hill, Inc.
- Jiang, G. L., Kohata, Y., Tateyama, M. and Tatsuoka, F. (1999). Small strain deformation characteristic at low pressure of dense gravel. *Proc. of 2nd Int. Symp. on Pre-Failure Deformation Characteristic of Geomaterials, IS Torino '99* (Jamiolkowski et al., eds.), Balkema, pp. 291-296,
- Kohata, Y., Jiang, G. L., Murata, O. & Tatsuoka, F. (1999). Elastic-properties-based modelling of non-linear deformation characteristics of gravels. *2nd Int. Symp. on Pre-Failure Deformation Characteristic of Geomaterials, IS Torino '99* (Jamiolkowski et al., eds.), Balkema, pp. 533-539.
- Kongsukprasert, L., Kuwano, R. and Tatsuoka, F. (2001). Effects of ageing with shear stress on the stress-strain behavior of cement-mixed sand. *Advanced Laboratory Stress-Strain Testing of Geomaterials* (Tatsuoka et al. eds.), Balkema, pp. 251-258.
- Kongsukprasert, L. and Tatsuoka, F. (2003). Viscous effects coupled with ageing effects on the stress-strain behaviour of cement-mixed granular materials and a model simulation, *Proc. 3rd Int. Symp. on Deformation Characteristics of Geomaterials, IS Lyon 03* (Di Benedetto et al. eds.), Balkema, pp. 569-577.
- Kongsukprasert, L., Tatsuoka, F. and Tateyama, M. (2005): Several factors affecting the strength and deformation characteristics of cement-mixed gravel, *Soils and Foundations* (accepted).
- Lohani, T. N., Kongsukprasert, L., Watanabe, K., and Tatsuoka, F. (2003a). Strength and deformation characteristics of cement-mixed gravel for engineering use. *Proc. 3rd Int. Symp. on Deformation Characteristics of Geomaterials, IS Lyon 03* (Di Benedetto et al. eds.), Balkema, 1. pp. 637-643.
- Lohani, T.N., Kongsukprasert, L., Watanabe, K. and Tatsuoka, F. (2003b). Strength and deformation properties of compacted cement-mixed gravel evaluated by triaxial compression tests. *Soils and Foundations*, Vol. 44, No. 5, pp. 95-108.
- Nakarai, K., Uchimura, T., Tatsuoka, F., Shinoda, M., Watanabe, K. and Tateyama, M. (2002). Seismic stability of geosynthetic-reinforced soil bridge abutment. *Proc. 7th Int. Conf. on Geosynthetics, IGS, Nice*, Vol. 1, pp. 249-252.
- Schrader, E.K. (1996). Compaction of roller compacted concrete. *SP96-6, ACI Special Publication*, pp. 77-101.
- Shinoda, M., Uchimura, T. and Tatsuoka, F. (2003a). Increasing the stiffness of mechanically reinforced backfill by preloading and prestressing. *Soils and Foundations*, Vol. 43, No. 1, pp. 75-92.
- Shinoda, M., Uchimura, T and Tatsuoka, F. (2003b). Improving the dynamic performance of preloaded and prestressed mechanically reinforced backfill by using a ratchet connection. *Soils and Foundations*, Vol. 43, No. 2, pp. 33-54.

- Sugai, M., Tatsuoka, F., Kuwabara, M. and Sugo, K. (2000). Strength and deformation characteristics of cement-mixed soft clay. *Coastal Geotechnical Engineering in Practice* (Nakase & Tsuchida eds.), Balkema, Vol. 1, pp. 521-527.
- Sugai, M. and Tatsuoka, F. (2003). Ageing and loading rate effects on the stress-strain behaviour of a cement-mixed soft clay, *Proc. 3rd Int. Sym. on Deformation Characteristics of Geomaterials*, IS Lyon 03 (Di Benedetto et al. eds.), Balkema, pp. 627-635.
- Tatsuoka, F., Uchida, K., Imai, K., Ouchi, T. and Kohata, Y. (1997a). Properties of cement-treated soils in Trans-Tokyo Bay Highway project. *Ground Improvement*, Thomas Telford, Vol. 1, No. 1, pp. 37-58.
- Tatsuoka, F., Uchimura, T. and Tateyama, M. (1997b). Preloaded and prestressed reinforced soil." *Soils and Foundations*, Vol. 37, No. 3, pp. 79-94.
- Tatsuoka, F., Tateyama, M., Uchimura, T. and Koseki, J. (1997c). Geosynthetic-reinforced soil retaining walls as important permanent structures. 1996-1997 Mercer Lecture, *Geosynthetic International*, Vol. 4, No. 2, pp. 81-136.
- Tatsuoka, F., Koseki, J., and Tateyama, M. (1997d). Performance of reinforced soil structures during the 1995 Hyogo-ken Nanbu Earthquake. Special Lecture, *Int. Sym. on Earth Reinforcement (IS Kyushu '96)*, Balkema, Vol. 2, pp. 973-1008.
- Tatsuoka, F., Uchida, K. and Ouchi, T. (2000). Geotechnical engineering aspects of Trans-Tokyo Bay Highway project. *Proc. GeoEng2000*, Melbourne, 1 (invited lectures), pp. 996-1024.
- Uchimura, T., Tateyama, M., Koga, T., and Tatsuoka, F. (2003). Performance of a preloaded-prestressed geogrid-reinforced soil pier for a railway bridge. *Soils and Foundations*, Vol. 43, No. 6, pp. 33-50.
- Watanabe, K., Tateyama, M., Yonezawa, T., Aoki, H., Tatsuoka, F. and Koseki, J. (2002). Shaking table tests on a new type bridge abutment with geogrid-reinforced cement treated backfill. *Proc. of 7th Int. Conf. on Geosynthetics*, IGS, Nice, Vol. 1, No. 119-122.
- Watanabe, K., Tateyama, M., Jiang, G., Tatsuoka, F., and Lohani, T. N., (2003a). Strength characteristics of cement-mixed gravel evaluated by large triaxial compression tests. *Proc. 3rd Int. Symp. on Deformation Characteristics of Geomaterials*, IS Lyon 03 (Di Benedetto et al. eds.), Balkema, pp. 683-693.
- Watanabe, O., Nasu, Y., Aoki, H., Yonezawa, T., Tateyama, M. and Tatsuoka, F. (2003b). Construction control of approach block of cement-mixed gravel backfill. *Proc. 58th Annual Conf. of JSCE, Tokushima, III*, pp. 1091-1092 (in Japanese).